PCCP

Strong Stretching Theory for pH-Responsive Polyelectrolyte Brushes in Large Salt Concentrations

Journal:	*Physical Chemistry Chemical Physics*
Manuscript ID	CP-ART-04-2020-002099
Article Type:	Paper
Date Submitted by the Author:	18-Apr-2020

Complete List of Authors:	Etha, Sai; University of Maryland, College Park, Mechanical Engineering Sivasankar, Vishal; University of Maryland, College Park, Mechanical Engineering Sachar, Harnoor; University of Maryland, College Park, Mechanical Engineering Das, Siddhartha; University of Maryland, College Park, Mechanical Engineering

Strong Stretching Theory for pH-Responsive Polyelectrolyte Brushes in Large Salt Concentrations

Sai Ankit Etha, Vishal Sankar Sivasankar, Harnoor Singh Sachar, and Siddhartha Das
Department of Mechanical Engineering, University of Maryland, College Park, MD-20742, USA
(Dated: April 18, 2020)

Abstract: In this paper, we develop a theory for describing the thermodynamics, configuration, and electrostatics of strongly-stretched, pH-responsive polyelectrolyte (PE) brushes in presence of large salt concentrations. The aim of the paper, therefore, is to study the properties of a PE brush in a salt concentration regime (namely large concentrations of several molars) that has been hitherto unexplored theoretically in the context of PE brushes, but can be routinely encountered in molecular scale simulations of the problem. The brushes are modelled using our recently developed augmented Strong Stretching Theory (SST), while the effect of the presence of the large salt concentration is accounted for by including the contributions of three different types of non-Poisson-Boltzmann (non-PB) effects in the free energy description of the PE brush induced electric double layer (EDL). These non-PB effects are ionic non-mean-field ion-ion correlations, solvent polarization, and finite size effect of the ions and water dipoles. We study the individual influences of these different effects and show that the ion-ion correlations and solvent polarization effect reduce the brush height and consequentially enhances the monomer density and leads to an electrostatic potential distribution of the brush induced EDL that has a larger magnitude at near-wall locations and becomes zero at shorter distances from the wall. The finite size effect, on the other hand, increases the brush height and therefore, weakens the monomer density and leads to a smaller near-wall magnitude of the EDL potential that becomes zero at larger distances from the wall. Eventually, we consider the impact of all the three non-PB effects simultaneously and show that the ion-ion correlation and solvent polarization effect dominate the size effects and dictate the overall brush configuration and the EDL electrostatics. We also point out that the influence of all the three non-PB effects becomes largest for larger salt concentration and smaller bulk pH. Finally, we compare our theoretical predictions with those obtained from our recently developed all-atom MD simulation model and obtain excellent match.

I. INTRODUCTION

Functionalizing surfaces by grafting them with charged polyelectrolyte (PE) molecules, in a manner such that they are tethered to the surface at close-enough proximity so as to form "brush"-like configurations, has been extensively employed for a large number of applications ranging from ion sensing [1, 2], sensing of biomolecules [3–5], fabricating current rectifiers [6] and nanofluidic diodes [7], ensuring colloid stabilization [8], developing novel techniques for oil recovery [9], water harvesting [10], and drug delivery [11], and many more. Several of these applications typically rely on the ability of these PE brushes to change their configurations as responses to the stimuli present in their environment (e.g., pH and the salt concentration of their surrounding fluidic medium). Also these applications, which are relatively recent, have renewed interest in better understanding the theoretical foundations dictating the thermodynamics, structure, and configuration of the PE brushes. Developing scaling laws, describing the brush height as functions of the various parameters PE brushes have formed a critical component of such theoretical approaches [12–19]. Also, much more detailed calculations, providing explicit description of the PE brush-induced electric double layers (EDLs) through Poisson-Boltzmann (PB) equations that can also account for the pH-responsiveness of the PE brushes, have been attempted for modelling the PE brushes [20–30]. These models also depend on the manner in which the brushes are described: i.e., through the use of the Alexander-de-Gennes model (that consider a constant monomer distribution along the length of the brush) [24–26], or the parabolic model [22, 27], or the strong stretching theory (SST) model [31–36], or the augmented SST (where the SST model is improved by accounting for the excluded volume interactions between the brush segments and an augmented form of the mass action law) [37, 38]. Most of these theoretical studies, however, do not consider the cases where the concentration of the salt in the medium is significantly large (i.e., several Molars). It is well established that for such large salt concentration, the standard Poisson-Boltzmann description of the electric double layer (EDL) breaks down [39–42] and one needs to account for the contributions of other non-Poisson-Boltzmann elements such as the finite ion size effect [39], solvent polarization effect [43], and the effect of ion-ion correlations [40, 41]. A recent all-atom molecular dynamics (MD) simulation study from our group [44] probing the behavior of the densely grafted PE brushes has shown that the concentration of the counterions surrounding the PE brushes can reach several molars/molals, confirming the need to develop a model to quantify the behavior of the PE brushes in presence of large salt concentration.

In this paper, we provide for the first time a complete theory describing the thermodynamics, configuration, and the electrostatics of the PE brushes in *large salt concentrations.* For this purpose, we invoke the recent theoretical model

of McEldrew *et al.* [42] for describing the thermodynamics of the electrolytes with very large salt concentrations (or effectively, the free energy of the EDL induced by the PE brushes). This study by McEldrew *et al.* [42], which accounts for three different non-Poisson-Boltzmann (non-PB) effects (namely, the ionic non-mean-field ion-ion correlations, the solvent polarization, and the finite size effect of the ions and water dipoles) is intended to model the water-in-salt electrolyte (WISE) systems. In such WISE systems, the added salt is present in such a large concentration that it outnumbers water by both weight and volume [45, 46]. The model proposed by McEldrew *et al.* [42] was developed from the prior theoretical studies on ionic liquids [41, 47, 48]. On the other hand, the PE brushes are described by our recently proposed augmented SST model [37, 38]. The augmented SST model improves the widely employed SST model for the PE brushes [31–36] by accounting for two additional effects, namely (a) the excluded volume interactions between the PE brush segments and (b) an expanded form of the mass action law that allows the PE chargeable site density to take different values (and not just a fixed value as in the case of the SST model). These two approaches, one for describing the electrolyte with large salt concentration and another for describing the PE brushes, are integrated to obtain a semi-analytically tractable free energy functional describing the PE brushes in large salt concentration. This functional is subsequently minimized to obtain the governing equations that provide a thermodynamically self-consistent and coupled description of the PE brush configuration (PE brush height and PE monomer distribution) and the electrostatics of the PE brush induced EDL for the case where the PE brushes are in a large salt concentration. A few prior studies had attempted to incorporate the effect of the mean-field non-PB factors (e.g., finite ion size effect or the solvent polarization effect) in description of the PE brushes [50, 51]; however, these studies suffered from considering a very primitive description of the PE brushes (for example, the brush-free energies have been totally neglected in these studies).

In our results, we first show the individual influence of the three different non-PB effects in the brush configuration (brush height and the brush monomer distribution) and the electrostatics of the brush-induced EDL. The ion-ion correlation effect tends to create local electroneutrality around the brushes: this reduces the bush inter-segmental repulsion thereby reducing the brush height. The solvent polarization effect, on the other hand, causes additional screening of the PE charge by ensuring a preferential alignment of the water dipoles: this effect too, therefore, reduces the PE-brush inter-segmental repulsion and hence decreases the brush height. Since the brush height reduces for the cases considering ion-ion correlations and solvent polarization effect, the monomer density increases and the EDL electrostatic potential shows a large magnitude at near-wall locations and becomes zero at much shorter distances from the wall. On the other hand, the consideration of the finite size effect leads to a smaller available space for the counterions thereby lowering their entropy; this enforces the brushes, in order to counter this effect, to stretch out more (i.e., the brush height increases) so as to provide a larger volume to the counterions. Accordingly, with the finite size effect, the monomer density decreases and the EDL electrostatic potential shows a smaller magnitude at near-wall locations and becomes zero at much greater distances from the wall. Finally, we consider all the three effects simultaneously and establish that for the chosen system parameters, the effects of the ion-ion correlation and solvent polarization overwhelm the effect of the finite sizes and therefore the brush configuration and the EDL electrostatics obey the same behavior as witnessed for the cases where the ion-ion correlation and solvent polarization effects are considered. We also point out that the effects of these non-PB factors are maximum for the cases of large salt concentration and small bulk pH. Furthermore, we demonstrate that for the cases of *smaller salt concentration*, the present model recovers the prediction of that of the augmented SST model [37] that does not consider the effect of large salt concentration. Finally, we compare the findings from the present model with those obtained from our recent all-atom MD simulation study [44] probing the behavior of densely grafted PE brushes in presence of large concentration of the ions (counterions) and achieve an excellent match. Overall, to the best of our knowledge, this study provides the first theory for the behavior of the strongly-stretched PE brushes in large salt concentration.

II. THEORETICAL FORMULATION

We consider pH-responsive, polyelectrolyte (PE) brushes present in a highly concentrated electrolytic solution. The PE molecules are grafted to a planar substrate with a small-enough lateral separation ($\ell = 30nm$ between the adjacent grafted PE chains) that ensure that the PE molecules attain a "brush"-like configuration, as shown in Fig. 1. In this study, we attempt to develop for the first time a theoretical model for the the thermodynamics, configuration, and the electrostatics of the PE brushes in such large salt concentration. Accordingly, our model will combine the formulation of McEldrew et al. [42] (who employed the asymmetric lattice model for studying the thermodynamics of large-concentration electrolytes) and our recently developed augmented SST for the PE brushes [37].

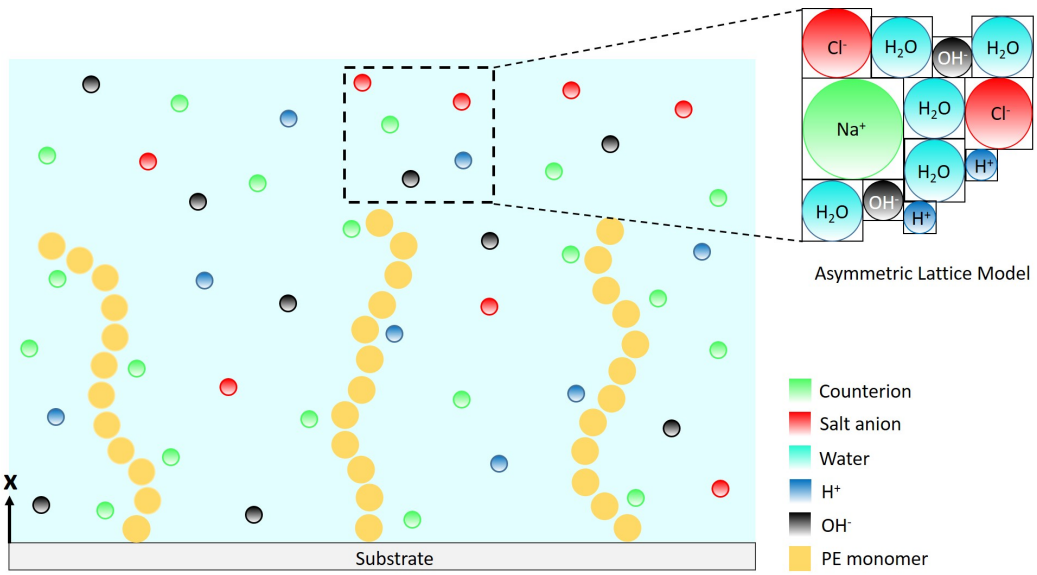

FIG. 1: Schematic representing the PE brush grafted on a planar substrate. We employ an asymmetric lattice model to describe the thermodynamics of the mobile ions and solvent dipoles.

We start by expressing the grand canonical free energy functional (Ω) of the system (assuming that the system is in a thermal and a chemical equilibrium with the bulk),

$$\Omega = \int_V \left(f_e + f_{brush} + f_{ion} - \sum_i n_i \mu_i \right) \, dV, \tag{1}$$

where V is the volume, f_e is the electrostatic energy density associated with the electric field developed around the charged PE brushes, f_{brush} is the PE brush free energy density, f_{ion} is the free energy density of all the mobile ionic species surrounding the PE brushes, n_i (i=+, −, H^+, OH^-, and w, representing the electrolyte cation, electrolyte anion, H^+ ion, OH^- ion, and water dipoles, respectively) is the number density of the mobile species i, and μ_i is the corresponding chemical potential (obtained from the chemical configuration of the bulk). As a next step, following McEldrew et al. [42], we make use of the Legendre transform for replacing the free energy density of the mobile ions and water dipoles and the contribution due to their chemical potentials with an equivalent thermodynamic pressure (P) as:

$$P = \sum_i n_i \mu_i - f_{ion}. \tag{2}$$

As a result, eq.(1) reduces to:

$$\Omega = \int_V \left(f_e + f_{brush} - P \right) \, dV. \tag{3}$$

Henceforth, we shall consider that there is no variation of any quantity parallel to the planar substrate. Therefore, the above integral gets expressed as:

$$\Omega = A \int \left(f_e + f_{brush} - P \right) \, dx, \tag{4}$$

where A is the area of the substrate and x denotes the direction perpendicular to the substrate. Below, we shall derive the expressions of the individual free energy (or free energy density) terms.

Electrostatic free energy of the electric field developed around the PE brush system
This differential form of this energy (δF_e) can be expressed in terms of the corresponding free energy density (f_e) as:

$$\delta F_e = \delta \int_V f_e \, dV = \int_V \boldsymbol{E} \cdot \delta \boldsymbol{D} \, dV, \tag{5}$$

where $\mathbf{E} = -\nabla\psi$ (ψ is the induced EDL electrostatic potential) and $\mathbf{D}$ are the electric field and the displacement field, respectively. Following McEldrew et al. [42], one can express the displacement field as:

$$\boldsymbol{D} = \varepsilon_0\varepsilon_r\boldsymbol{E} + \boldsymbol{P}_{pol} + \boldsymbol{P}_{BSK}, \tag{6}$$

where, ε_0 is the permittivity of vacuum, ε_r is the permittivity of the solvent, $\mathbf{P}_{pol}$ represents the contribution associated with the polarization of the dipoles in the developed electric field, and $\mathbf{P}_{BSK}$ (described by the Bazant-Storey-Kornyshev theory [41]) is the contribution associated with the polarization field induced by the presence of the correlated ions in the system. $\mathbf{P}_{pol}$ and $\mathbf{P}_{BSK}$ can be expressed as [42]:

$$\mathbf{P}_{pol} = n_w p_w \mathcal{L}(\beta p_w \boldsymbol{E}), \tag{7}$$

$$\mathbf{P}_{BSK} = -\varepsilon_0\varepsilon_r l_c^2 \nabla^2 \boldsymbol{E}, \tag{8}$$

where n_w is the number density of the water dipoles, p_w is the dipolar moment of the free dipoles, (L) is the Langevin function, $\beta = \frac{1}{k_B T}$ is the inverse of thermal energy, and l_c is a lengthscale associated with the ion-ion correlations effect [41]. Finally, using eqs.(6,7,8) in eq.(5) and obtaining a variational integral of δF_e from 0 to F_e under the constraint $\nabla \cdot \boldsymbol{D} = \rho_e$ [where $\rho_e = e(n_+ - n_- + n_{H^+} - n_{OH^-})$ is the volume charge density of mobile ions], we can write (the detailed steps are provided in McEldrew et al. [42]; we repeat them in Appendix A for the ease of understanding of the readers):

$$F_e = \int_V f_e dV = \int_V \left[\rho_e\psi - \frac{\varepsilon_0\varepsilon_r}{2}(|\nabla\psi|^2 + l_c^2|\nabla^2\psi|^2) - \frac{n_w}{\beta}\ln\left(\frac{sinh(\beta p_w \nabla\psi)}{\beta p_w \nabla\psi}\right)\right] dV. \tag{9}$$

Expression for the thermodynamic pressure P defined in eq.(2)

For obtaining the thermodynamic pressure function (P) of the electrolyte system, we consider an asymmetric lattice model for the electrolyte [42]. Accordingly, we use a grand canonical partition function to represent a 5-component system (4 species of mobile ions and water)

$$\Xi = \sum_{\chi_+=0}^{\infty}\sum_{\chi_-=0}^{\infty}\sum_{\chi_{H^+}=0}^{\infty}\sum_{\chi_{OH^-}=0}^{\infty}\sum_{\chi_w=0}^{\infty} e^{\beta\mu_+\chi_+}e^{\beta\mu_-\chi_-}e^{\beta\mu_{H^+}\chi_{H^+}}e^{\beta\mu_{OH^-}\chi_{OH^-}}e^{\beta\mu_w\chi_w}Q(\chi_+)Q(\chi_-)Q(\chi_{H^+})Q(\chi_{OH^-})Q(\chi_w). \tag{10}$$

Here, Q represents the canonical partition function of each species, and can be expressed as, $Q(\chi_j) = \omega_j e^{-\beta\epsilon_j\chi_j}$, with the energy given by $E_j = \epsilon_j\chi_j$ [42] and χ_j represents the number of lattice sites occupied by species j. In line with the models of Han et al. [49] and McEldrew et al. [42], we assume that the different species/components fill the lattice in a manner such that the configuration of each species is equivalent to the occupation of χ_j lattice sites out of a total of N_t available sites (per unit volume), so that $\omega_j = \frac{N_t!}{\chi_j!(N_t-\chi_j)!}$. Finally, using the fact that the pressure P in a grand canonical ensemble is related to the partition function as, $PV_L = k_B T ln\Xi$ (where $V_L = N_t v_{H^+}$ is the total available lattice volume), we can obtain (see Appendix B for the detailed derivation):

$$P = \frac{k_B T}{v_{H^+}} ln\left[\left(\left(\left(\left\{1+\xi_{OH^-}e^{\beta\tilde{\mu}_{OH^-}}\right\}^{\xi_{H^+}/\xi_{OH^-}} + \xi_{H^+}e^{\beta\tilde{\mu}_{H^+}}\right)^{\xi_+/\xi_{H^+}} + \xi_+ e^{\beta\tilde{\mu}_+}\right)^{\xi_-/\xi_+} + \xi_- e^{\beta\tilde{\mu}_-}\right)^{\xi_w/\xi_-} + \xi_w e^{\beta\tilde{\mu}_w}\right]^{1/\xi_w}, \tag{11}$$

where, $\xi_j = v_j\ /v_{H^+}$ (v_j is the volume of an individual element of species j and we non-dimensionalize with the volume of smallest species, v_{H^+}) and $\tilde{\mu}_j = \mu_j - \epsilon_j$.

Expression for the free energy of the PE brushes

Here we describe the brushes following our newly developed augmented Strong Stretching Theory (SST) model (see our previous paper [37] for the detailed derivation). Here we repeat the key equations for the sake of continuity. The total free energy associated with the PE brushes can be expressed as:

$$\int_V f_{brush}\ dV = \int_V \left(f_{els} + f_{EV} + f_{brush,ion} + f_{brush,elec}\right) dV, \tag{12}$$

where f_{els} is the elastic free energy of the brush, f_{EV} is the excluded volume free energy of the brush, $f_{brush,ion}$ is the free energy of the brush associated with its degree of ionization, and $f_{brush,elec}$ is the electrostatic free energy associated with the charges on the brush. We consider a SST description, where the electrostatic repulsion between the charged monomers of the PE brushes ensures that the PE chains are strongly stretched. We consider the equilibrium brush height H to be the maximum height of the PE monomers from the substrate. Additionally, the system is divided into two regions: the interior of the brush ($0 \leq x \leq H$) comprising of all the PE molecules and the exterior to the brush ($H < x \leq \infty$). Hence, using the notation of Zhulina et al. [52], we can write:

$$\int_V f_{els}\ dV = \frac{3k_BT}{2pa^2}\int_0^H g(x')dx' \int_0^{x'} E(x,x')dx, \tag{13}$$

$$\int_V f_{EV}\ dV = \frac{k_BT\sigma}{a^3}\int_0^H f_{conc}[\phi(x)]dx, \tag{14}$$

where, $E(x,x') = \frac{dx}{dn}$ is the elastic stretching of a PE chain at a distance x from the substrate and whose end is located at the coordinate x'. The quantities p, σ and a are the chain rigidity, the grafted area per chain (ℓ^2) and the Kuhn length of the PE chain, respectively. Also, $\phi(x)$ is the monomer distribution profile of a PE chain, and $f_{conc}[\phi(x)]$ is the non-dimensionalised free energy contribution from the excluded volume interactions, per unit volume. Finally, $g(x')$ is the normalized distribution function of the PE chain ends, defined as:

$$\int_0^H g(x')\ dx' = 1. \tag{15}$$

Furthermore, we can express $f_{brush,elec}$ as:

$$\int_V f_{brush,elec}\ dV = -\sigma\int_0^H e\psi n_{A^-}\phi\ dx, \tag{16}$$

where n_{A^-} represents the local number density of the PE charge, e is the electronic charge, and ψ is the electrostatic potential. Here, the negative sign indicates that the charge on the PE chains is negative. The negative charge on these PE chains is a result of the ionization of the PE chain of the form $HA \rightarrow H^+ + A^-$. Hence, n_{A^-} is a function of the H^+ ion number density (n_{H^+}) and will be derived later. Finally, following Zhulina and Borisov [31], we write the free energy of ionization of the brush molecules, based on mixing entropies of the protonated and deprotonated PE monomer units as well as energy of dissociation associated with the emergence of additional H^+ ions, as:

$$\begin{aligned}
&\int_V f_{brush,ion}\ dV = \frac{k_BT\sigma}{a^3}\int_0^H \phi\left[\left(1-\tfrac{n_{A^-}}{\gamma}\right)ln\left(1-\tfrac{n_{A^-}}{\gamma}\right) + \tfrac{n_{A^-}}{\gamma}ln\left(\tfrac{n_{A^-}}{\gamma}\right) + \tfrac{n_{A^-}}{\gamma}\left(\tfrac{\mu^0_{H^+}+\mu^0_{A^-}-\mu^0_{AH}}{k_BT} + ln(n_{H^+,\infty})\right)\right]dx \\
\implies &\int_V f_{brush,ion}\ dV = \frac{k_BT\sigma}{a^3}\int_0^H \phi\left[\left(1-\frac{n_{A^-}}{\gamma}\right)ln\left(1-\frac{n_{A^-}}{\gamma}\right) + \frac{n_{A^-}}{\gamma}ln\left(\frac{n_{A^-}}{\gamma}\right) + \frac{n_{A^-}}{\gamma}ln\left(\frac{n_{H^+,\infty}}{K'_a}\right)\right]dx,
\end{aligned} \tag{17}$$

where, K_a is the ionization constant of the PE monomer ionization reaction $HA \rightarrow H^+ + A^-$, N_A is the Avogadro number and $K'_a = 10^3 N_A K_a$. The dissociation constant, $K_a = \exp\left(-\frac{\mu^0_{H^+}+\mu^0_{A^-}-\mu^0_{AH}}{k_BT}\right)$, where μ^0_i represents the standard chemical potential of species i. Also, $n_{H^+,\infty} = 10^{3-pH_\infty}N_A$ is the bulk number density of the H^+ ions (pH_∞ is the bulk pH) and γ ($1/m^3$) is the density of chargeable sites on the PE chains.
Therefore, using eqs.(13,14,16,17) in eq. (12) we can obtain the overall free energy of the brush as:

$$\begin{aligned}
\int_V f_{brush}\ dV = &\ \frac{3k_BT}{2pa^2}\int_0^H g(x')dx'\int_0^{x'} E(x,x')dx\ +\ \frac{k_BT\sigma}{a^3}\int_0^H f_{conc}[\phi(x)]dx\ -\ \sigma\int_0^H e\psi n_{A^-}\phi\ dx \\
&+ \frac{k_BT\sigma}{a^3}\int_0^H \phi\left[\left(1-\frac{n_{A^-}}{\gamma}\right)ln\left(1-\frac{n_{A^-}}{\gamma}\right) + \frac{n_{A^-}}{\gamma}ln\left(\frac{n_{A^-}}{\gamma}\right) + \frac{n_{A^-}}{\gamma}ln\left(\frac{n_{H^+,\infty}}{K'_a}\right)\right]dx.
\end{aligned} \tag{18}$$

Finally, we should point out that the free energy of the brushes should be obtained in the presence of two constraints expressed as:

$$N = \int_0^{x'}\frac{dx}{E(x,x')}, \tag{19}$$

$$N = \frac{\sigma}{a^3}\int_0^H \phi(x)dx, \tag{20}$$

where N is the number of monomers per chain.

Final expression of the grand canonical free energy functional Ω expressed in eq.(4)
Using eqs.(9,11,18,19,20) in eq.(4), we get the final expression for the grand canonical free energy functional Ω as:

$$\begin{aligned}\Omega = A\int_V \Bigg[e\psi(n_+ - n_- + n_{H^+} - n_{OH^-}) - \frac{\varepsilon_0\varepsilon_r}{2}(|\nabla\psi|^2 + l_c^2|\nabla^2\psi|^2) - \frac{n_w}{\beta}\ln\left(\frac{sinh(\beta p_w\nabla\psi)}{\beta p_w\nabla\psi}\right) - P\Bigg]\, dx \\ + \frac{3k_BT}{2pa^2}\int_0^H g(x')dx'\int_0^{x'} E(x,x')dx \;+\; \frac{k_BT\sigma}{a^3}\int_0^H f_{conc}[\phi(x)]dx \;-\; \sigma\int_0^H e\psi n_{A^-}\phi\, dx \\ + \frac{k_BT\sigma}{a^3}\int_0^H \phi\Bigg[\Big(1-\frac{n_{A^-}}{\gamma}\Big)ln\Big(1-\frac{n_{A^-}}{\gamma}\Big) + \frac{n_{A^-}}{\gamma}ln\Big(\frac{n_{A^-}}{\gamma}\Big) + \frac{n_{A^-}}{\gamma}ln\Big(\frac{n_{H^+,\infty}}{K_a'}\Big)\Bigg]dx \\ + \lambda_1\Big[\frac{\sigma}{a^3}\int_0^H \phi(x)dx - N\Big] + \int_0^H \lambda_2(x')dx'\Big[\int_0^{x'}\frac{dx}{E(x,x')} - N\Big],\end{aligned} \tag{21}$$

where λ_2 and λ_1 serve as the Lagrange multipliers accounting for the constraints expressed in eq.(19) and eq.(20), respectively.

Minimization Procedure
In order to get the differential equations governing the problem, we first need to find the PE brush equilibrium state. For that purpose, we employ variational calculus and minimize the free energy terms for the PE brushes (w.r.t $E(x,x')$, $g(x')$, and n_{A^-}) in eq.(21). This minimization (the procedure has been described in detail in our previous paper [37] as well as in the Appendix C) yields:

$$E(x,x') = \frac{\pi}{2N}\sqrt{x'^2 - x^2}, \tag{22}$$

$$\begin{aligned}\int_0^{x'}\Bigg[\frac{3E(x,x')}{2a^2} + \Bigg(\frac{\delta f_{conc}}{\delta\phi} + \lambda_1 - \frac{ea^3\psi}{k_BT}n_{A^-} + \Big(1-\frac{n_{A^-}}{\gamma}\Big)ln\Big(1-\frac{n_{A^-}}{\gamma}\Big) + \frac{n_{A^-}}{\gamma}ln\Big(\frac{n_{A^-}}{\gamma}\Big) \\ + \frac{n_{A^-}}{\gamma}ln\Big(\frac{n_{H^+,\infty}}{K_a'}\Big)\Bigg)\frac{1}{E(x,x')}\Bigg]dx = 0,\end{aligned} \tag{23}$$

$$n_{A^-} = \frac{K_a'\gamma}{K_a' + n_{H^+,\infty}\exp\big(-\gamma a^3\frac{e\psi}{k_BT}\big)}, \tag{24}$$

$$\begin{aligned}\phi(x) = &\frac{\nu}{3\omega}\Bigg[\Bigg\{1 + \kappa^2\Bigg(\lambda_3 - x^2 + \alpha\frac{K_a'\gamma}{K_a' + n_{H^+,\infty}\exp\big(-\gamma a^3\frac{e\psi}{k_BT}\big)}\psi \\ &-\rho\Big(1 - \frac{K_a'}{K_a' + n_{H^+,\infty}\exp\big(-\gamma a^3\frac{e\psi}{k_BT}\big)}\Big)ln\Big(1 - \frac{K_a'}{K_a' + n_{H^+,\infty}\exp\big(-\gamma a^3\frac{e\psi}{k_BT}\big)}\Big) \\ &-\rho\frac{K_a'}{K_a' + n_{H^+,\infty}\exp\big(-\gamma a^3\frac{e\psi}{k_BT}\big)}ln\Big(\frac{K_a'}{K_a' + n_{H^+,\infty}\exp\big(-\gamma a^3\frac{e\psi}{k_BT}\big)}\Big) \\ &-\rho\frac{K_a'}{K_a' + n_{H^+,\infty}\exp\big(-\gamma a^3\frac{e\psi}{k_BT}\big)}ln\Big(\frac{n_{H^+,\infty}}{K_a'}\Big)\Bigg)\Bigg\}^{1/2} - 1\Bigg].\end{aligned} \tag{25}$$

In eq.(25), $\kappa^2 = \frac{9\pi^2\omega_0}{8N^2pa^2\nu_0^2}$, $\rho = \frac{8a^2N^2p}{3\pi^2}$, $\lambda_3 = -\lambda_1\rho = -\lambda_1\frac{8a^2N^2p}{3\pi^2}$, and $\alpha = \frac{8N^2epa^5}{3\pi^2k_BT}$. Also, it is useful to note (as has been explained in details in Appendix C), to obtain eq.(25), we use the following virial expansion of f_{conc}:

$$f_{conc}[\phi(x)] \approx \nu_0\phi^2 + \omega_0\phi^3 + \dots, \tag{26}$$

where ν_0 and ω_0 are the virial coefficients.

We now, have all variables in terms of ψ (except the equilibrium brush height, H_0 and the Lagrange multiplier, λ_3). Hence, all of this culminates with the governing equation for the ψ, that is obtained by taking the variation of eq.(21) with respect to ψ and setting it to zero, yielding (with $\psi' = d\psi/dx$):

$$\epsilon_0\epsilon_r\Big(1 - l_c^2\frac{d^2}{dx^2}\Big)\frac{d^2\psi}{dx^2} + \frac{d}{dx}\left(n_w p_w \mathcal{L}(\beta p_w \psi')\right) + e\Bigg(n_+ - n_- + n_{H^+} - n_{OH^-}$$
$$- \frac{K_a'\gamma}{K_a' + n_{H^+,\infty}\exp\big(-\gamma a^3\frac{e\psi}{k_BT}\big)}\frac{\nu}{3\omega}\Bigg[\Bigg\{1 + \kappa^2\Bigg(\lambda_3 - x^2 + \alpha\frac{K_a'\gamma}{K_a' + n_{H^+,\infty}\exp\big(-\gamma a^3\frac{e\psi}{k_BT}\big)}\psi$$
$$-\rho\Big(1 - \frac{K_a'}{K_a' + n_{H^+,\infty}\exp\big(-\gamma a^3\frac{e\psi}{k_BT}\big)}\Big)ln\Big(1 - \frac{K_a'}{K_a' + n_{H^+,\infty}\exp\big(-\gamma a^3\frac{e\psi}{k_BT}\big)}\Big)$$
$$-\rho\frac{K_a'}{K_a' + n_{H^+,\infty}\exp\big(-\gamma a^3\frac{e\psi}{k_BT}\big)}ln\Big(\frac{K_a'}{K_a' + n_{H^+,\infty}\exp\big(-\gamma a^3\frac{e\psi}{k_BT}\big)}\Big)$$
$$-\rho\frac{K_a'}{K_a' + n_{H^+,\infty}\exp\big(-\gamma a^3\frac{e\psi}{k_BT}\big)}ln\Big(\frac{n_{H^+,\infty}}{K_a'}\Big)\Bigg)\Bigg\}^{1/2} - 1\Bigg]\Bigg) = 0 \qquad (0 \le x \le H),$$

$$\epsilon_0\epsilon_r\Big(1 - l_c^2\frac{d^2}{dx^2}\Big)\frac{d^2\psi}{dx^2} + \frac{d}{dx}\left(n_w p_w \mathcal{L}(\beta p_w \psi')\right) + e\left(n_+ - n_- + n_{H^+} - n_{OH^-}\right) = 0 \qquad (H \le x \le \infty). \tag{27}$$

To solve these ODE's we need to first find an expression for the number density (n_j) of each of the mobile species (we already have the concentration of the PE charge, n_{A^-}). For this purpose, we shall use $n_j = \frac{\partial P}{\partial \mu_j}\Big|_{T,\mu_{i\neq j}}$. [where P is defined in eq.(11)], yielding:

$$\begin{aligned}
n_w &= \frac{1}{v_{H^+}}\frac{e^{\beta(\mu_w+\Lambda)}}{D_1},\\
n_- &= \frac{1}{v_{H^+}}\frac{e^{\beta(\mu_- + e\psi)}(D_2)^{\xi_w/\xi_- - 1}}{D_1},\\
n_+ &= \frac{1}{v_{H^+}}\frac{e^{\beta(\mu_+ - e\psi)}(D_2)^{\xi_w/\xi_- - 1}(D_3)^{\xi_-/\xi_+ - 1}}{D_1},\\
n_{H^+} &= \frac{1}{v_{H^+}}\frac{e^{\beta(\mu_{H^+} - e\psi)}(D_2)^{\xi_w/\xi_- - 1}(D_3)^{\xi_-/\xi_+ - 1}(D_4)^{\xi_+/\xi_{H^+} - 1}}{D_1},\\
n_{OH^-} &= \frac{1}{v_{H^+}}\frac{e^{\beta(\mu_{OH^-} + e\psi)}(D_2)^{\xi_w/\xi_- - 1}(D_3)^{\xi_-/\xi_+ - 1}(D_4)^{\xi_+/\xi_{H^+} - 1}(D_5)^{\xi_{H^+}/\xi_{OH^-} - 1}}{D_1}.
\end{aligned} \tag{28}$$

In the above equations, $\Lambda = k_BTln(sinh(\beta p_w\psi')/\beta p_w\psi')$ is the free energy associated with the dipolar fluctuations in an electric field and

$$\begin{aligned}
D_5 &= 1 + \xi_{OH^-}e^{\beta(\mu_{OH^-} + e\psi)},\\
D_4 &= D_5^{\xi_{H^+}/\xi_{OH^-}} + \xi_{H^+}e^{\beta(\mu_{H^+} - e\psi)},\\
D_3 &= D_4^{\xi_+/\xi_{H^+}} + \xi_+e^{\beta(\mu_+ - e\psi)},\\
D_2 &= D_3^{\xi_-/\xi_+} + \xi_-e^{\beta(\mu_- + e\psi)},\\
D_1 &= D_2^{\xi_w/\xi_-} + \xi_we^{\beta(\mu_w + \Lambda)}.
\end{aligned} \tag{29}$$

To use the above equations, we need to know the values of the chemical potential of the mobile species, μ_j. This is

obtained by forcing the ion distributions to be equal to the bulk concentrations in the limit of $x \to \infty$, yielding:

$$
\begin{aligned}
\mu_{OH^-} =\ & \frac{1}{\beta} ln \left[\frac{n_{OH^-,\infty} v_{H^+}}{1-\xi_w n_{w,\infty} v_{H^+} - \xi_- n_{-,\infty} v_{H^+} - \xi_+ n_{+,\infty} v_{H^+} - \xi_{H^+} n_{H^+,\infty} v_{H^+} - \xi_{OH^-} n_{OH^-,\infty} v_{H^+}} \right], \\
\mu_{H^+} =\ & \frac{1}{\beta} ln \left[\frac{n_{H^+,\infty} v_{H^+}}{1-\xi_w n_{w,\infty} v_{H^+} - \xi_- n_{-,\infty} v_{H^+} - \xi_+ n_{+,\infty} v_{H^+} - \xi_{H^+} n_{H^+,\infty} v_{H^+}} \right] + \\
& \frac{\xi_{H^+}}{\xi_{OH^-}} ln \left[\frac{1-\xi_w n_{w,\infty} v_{H^+} - \xi_- n_{-,\infty} v_{H^+} - \xi_+ n_{+,\infty} v_{H^+} - \xi_{H^+} n_{H^+,\infty} v_{H^+}}{1-\xi_w n_{w,\infty} v_{H^+} - \xi_- n_{-,\infty} v_{H^+} - \xi_+ n_{+,\infty} v_{H^+} - \xi_{H^+} n_{H^+,\infty} v_{H^+} - \xi_{OH^-} n_{OH^-,\infty} v_{H^+}} \right], \\
\mu_{+} =\ & \frac{1}{\beta} ln \left[\frac{n_{+,\infty} v_{H^+}}{1-\xi_w n_{w,\infty} v_{H^+} - \xi_- n_{-,\infty} v_{H^+} - \xi_+ n_{+,\infty} v_{H^+}} \right] + \\
& \frac{\xi_{+}}{\xi_{OH^-}} ln \left[\frac{1-\xi_w n_{w,\infty} v_{H^+} - \xi_- n_{-,\infty} v_{H^+} - \xi_+ n_{+,\infty} v_{H^+} - \xi_{H^+} n_{H^+,\infty} v_{H^+}}{1-\xi_w n_{w,\infty} v_{H^+} - \xi_- n_{-,\infty} v_{H^+} - \xi_+ n_{+,\infty} v_{H^+} - \xi_{H^+} n_{H^+,\infty} v_{H^+} - \xi_{OH^-} n_{OH^-,\infty} v_{H^+}} \right] + \\
& \frac{\xi_{+}}{\xi_{H^+}} ln \left[\frac{1-\xi_w n_{w,\infty} v_{H^+} - \xi_- n_{-,\infty} v_{H^+} - \xi_+ n_{+,\infty} v_{H^+}}{1-\xi_w n_{w,\infty} v_{H^+} - \xi_- n_{-,\infty} v_{H^+} - \xi_+ n_{+,\infty} v_{H^+} - \xi_{H^+} n_{H^+,\infty} v_{H^+}} \right], \\
\mu_{-} =\ & \frac{1}{\beta} ln \left[\frac{n_{-,\infty} v_{H^+}}{1-\xi_w n_{w,\infty} v_{H^+} - \xi_- n_{-,\infty} v_{H^+}} \right] + \\
& \frac{\xi_{-}}{\xi_{OH^-}} ln \left[\frac{1-\xi_w n_{w,\infty} v_{H^+} - \xi_- n_{-,\infty} v_{H^+} - \xi_+ n_{+,\infty} v_{H^+} - \xi_{H^+} n_{H^+,\infty} v_{H^+}}{1-\xi_w n_{w,\infty} v_{H^+} - \xi_- n_{-,\infty} v_{H^+} - \xi_+ n_{+,\infty} v_{H^+} - \xi_{H^+} n_{H^+,\infty} v_{H^+} - \xi_{OH^-} n_{OH^-,\infty} v_{H^+}} \right] + \\
& \frac{\xi_{-}}{\xi_{H^+}} ln \left[\frac{1-\xi_w n_{w,\infty} v_{H^+} - \xi_- n_{-,\infty} v_{H^+} - \xi_+ n_{+,\infty} v_{H^+}}{1-\xi_w n_{w,\infty} v_{H^+} - \xi_- n_{-,\infty} v_{H^+} - \xi_+ n_{+,\infty} v_{H^+} - \xi_{H^+} n_{H^+,\infty} v_{H^+}} \right] + \\
& \frac{\xi_{-}}{\xi_{+}} ln \left[\frac{1-\xi_w n_{w,\infty} v_{H^+} - \xi_- n_{-,\infty} v_{H^+}}{1-\xi_w n_{w,\infty} v_{H^+} - \xi_- n_{-,\infty} v_{H^+} - \xi_+ n_{+,\infty} v_{H^+}} \right], \\
\mu_{w} =\ & \frac{1}{\beta} ln \left[\frac{n_{w,\infty} v_{H^+}}{1-\xi_w n_{w,\infty} v_{H^+}} \right] + \\
& \frac{\xi_{w}}{\xi_{OH^-}} ln \left[\frac{1-\xi_w n_{w,\infty} v_{H^+} - \xi_- n_{-,\infty} v_{H^+} - \xi_+ n_{+,\infty} v_{H^+} - \xi_{H^+} n_{H^+,\infty} v_{H^+}}{1-\xi_w n_{w,\infty} v_{H^+} - \xi_- n_{-,\infty} v_{H^+} - \xi_+ n_{+,\infty} v_{H^+} - \xi_{H^+} n_{H^+,\infty} v_{H^+} - \xi_{OH^-} n_{OH^-,\infty} v_{H^+}} \right] + \\
& \frac{\xi_{w}}{\xi_{H^+}} ln \left[\frac{1-\xi_w n_{w,\infty} v_{H^+} - \xi_- n_{-,\infty} v_{H^+} - \xi_+ n_{+,\infty} v_{H^+}}{1-\xi_w n_{w,\infty} v_{H^+} - \xi_- n_{-,\infty} v_{H^+} - \xi_+ n_{+,\infty} v_{H^+} - \xi_{H^+} n_{H^+,\infty} v_{H^+}} \right] + \\
& \frac{\xi_{w}}{\xi_{+}} ln \left[\frac{1-\xi_w n_{w,\infty} v_{H^+} - \xi_- n_{-,\infty} v_{H^+}}{1-\xi_w n_{w,\infty} v_{H^+} - \xi_- n_{-,\infty} v_{H^+} - \xi_+ n_{+,\infty} v_{H^+}} \right] + \\
& \frac{\xi_{w}}{\xi_{-}} ln \left[\frac{1-\xi_w n_{w,\infty} v_{H^+}}{1-\xi_w n_{w,\infty} v_{H^+} - \xi_- n_{-,\infty} v_{H^+}} \right].
\end{aligned}
\tag{30}
$$

where, $n_{j,\infty}$ represents the bulk number density of the species j.

In order to solve the governing ODEs, we need to know the boundary conditions for our problem. We use the following boundary conditions for ψ:

$$
(\psi)_{x=H^-} = (\psi)_{x=H^+},\ \left(\frac{d\psi}{dx}\right)_{x=H^-} = \left(\frac{d\psi}{dx}\right)_{x=H^+},\ \left(\frac{d\psi}{dx}\right)_{x=0} = 0,\ \left(\frac{d^3\psi}{dx^3}\right)_{x=0} = 0,\ (\psi)_{x\to\infty} = 0,\ \left(\frac{d^3\psi}{dx^3}\right)_{x\to\infty} = 0. \tag{31}
$$

The last thing we require is to find the equilibrium structure of the PE brushes themselves (equilibrium height H_0). This requires that we know λ_3, which can be obtained by substituting eq.(25) in eq.(20). Hence, we use the following procedure: For a given guess of the equilibrium height (H_0), we use our set of equations to obtain ϕ, ψ, and λ_3. This gives us the distribution of all charged species in our system (n_j), which can then be used to calculate the net charge

(q_{net}) in the system using $q_{net} = e\sigma \int_0^\infty (n_+ - n_- + n_{H^+} - n_{OH^-} - \phi n_{A^-})dx$. The true equilibrium brush height, H_0, can then be obtained by enforcing the condition that $(q_{net})_{H=H_0} = 0$.

III. RESULTS

Having established a more generic formulation for describing the thermodynamics, configuration, and electrostatics of the PE brushes in large salt concentrations, we now provide a few results to understand the effects of the different non-PB terms (employed to account for the effects of the large salt concentrations) on the electrostatics and the resulting brush structure. We first point out the effect of each of the non-PB effects individually (this is ensured by mathematically "turning on" only one of the non-PB effect at a time) on the PE brush structure (quantified by the brush height and the monomer distribution) and the induced EDL (characterized by the variation of the corresponding EDL electrostatic potential) and compare these results with those obtained from the case where the PE brushes are described by the augmented SST of Sachar et al. [37] without any non-PB term. Finally, we study the influence of all the different non-PB effects "turned on" simultaneously.

A. Effect of ion-ion correlation

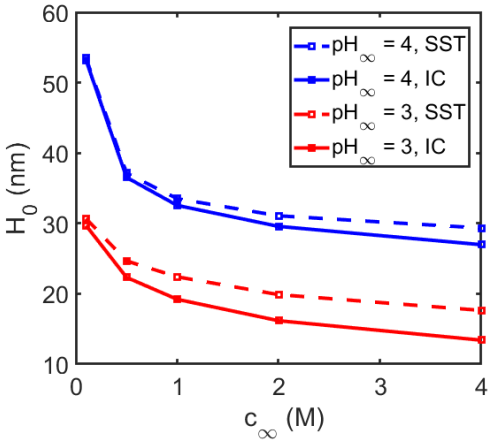

FIG. 2: Variation of the equilibrium brush height, H_0, with salt concentration (c_∞, expressed in M, with $c_\infty = n_\infty/(10^3 N_A)$ and n_∞ is the bulk number density of the salt having the units of $1/m^3$) for various pH_∞ values. Here, "IC" refers to the case where only the ion-ion correlations, among the different non-PB effects, have been accounted for to describe the EDL electrostatics, while the PE brushes are described using the augmented SST [37]. On the other hand, "SST" refers to the case where the EDL electrostatics is modelled using the standard PB model (i.e., we consider no non-PB term) and the PE brushes are modelled using the augmented SST [37]. Parameters used in this work are $k_B = 1.38 \times 10^{-23} J/K$, $T = 300K$, $pK_a = 3.5$, $a = 1nm$, $\ell = 30nm$, $\gamma = 1/a^3$ (1 polyelectrolyte chargeable site per Kuhn monomer), $N = 400$, $pK_w = 14$, $p = 1$, $\nu_0 = 0.5$, $\omega_0 = 0.1$, $e = 1.6 \times 10^{-19} C$, $\epsilon_0 = 8.854 \times 10^{-12} F/m$, $\epsilon_r = 79.8$, $pOH_\infty = pK_w - pH_\infty$, $n_{+,\infty} = n_\infty$, $n_{H^+,\infty} = 10^3 N_A 10^{-pH_\infty}$, $n_{OH^-,\infty} = 10^3 N_A 10^{-pOH_\infty}$, $n_{-,\infty} = n_\infty + n_{H^+,\infty} - n_{OH^-,\infty}$, $n_{w,\infty} = 10^3 N_A (1000\rho_w - 58.44 c_\infty)/18$, where ρ_w is the density (in g/cc) of the bulk electrolyte salt solution and is expressed as a function of the salt concentration [53], and $l_c = 0.3\ nm$.

We first investigate the effect of the ion-ion correlations (IC) on the brush configuration and the induced EDL electrostatics. The extent of influence of these interactions are determined by the length scale l_c dictating the correlation. In our case, since we consider relatively large salt concentrations, we chose l_c to be of the order of the radius of the ions that are correlated. We choose NaCl as the salt; accordingly, we choose $l_c = 0.3\ nm$, which is similar to the size of the first hydration shell of these ions species [54, 55]. Fig. 2 shows the variation of equilibrium PE brush height with the bulk salt concentration for two different bulk values of pH: 3 and 4. The brush height decreases in presence of ion-ion correlations and the extent of this decrease becomes more severe at larger salt concentration and smaller bulk pH (or pH_∞). Ion-ion correlations tend to create local electroneutrality around the charged segments of the PE brush owing to the localization of more counterions near the brush segments. This leads to effectively lower inter-segmental electrostatic repulsions in the brushes over longer distances ($\sim$ greater than Kuhn length) causing a shorter brush height. At larger salt concentration, there are more counterions localized near the brushes: the ion-ion correlation effect affects a larger number of ions in the vicinity of the brushes triggering a more enhanced

electroneutrality effect. This justifies why the effect of ion-ion correlation in reducing the brush height (for a given pH_∞) is more prominent at a larger salt concentration. On the other hand, for a smaller pH_∞, there is a larger concentration of H^+ ions both in the bulk as well as near the PE brushes; therefore, the ion-ion correlation effect now acts on a larger number of H^+ ions. Hence the ion-ion correlation induced creation of local electroneutrality effect in the vicinity of the brushes becomes more prominent for a smaller pH_∞ at a given value of salt concentration, leading to a more prominent decrease in the brush height. Also, for a larger pH_∞, the brush is almost completely ionized, which implies that the effect of brush ionization is quite large as compared to the ion-ion correlations thereby reducing the difference between the cases of with and without the ion-ion correlation.

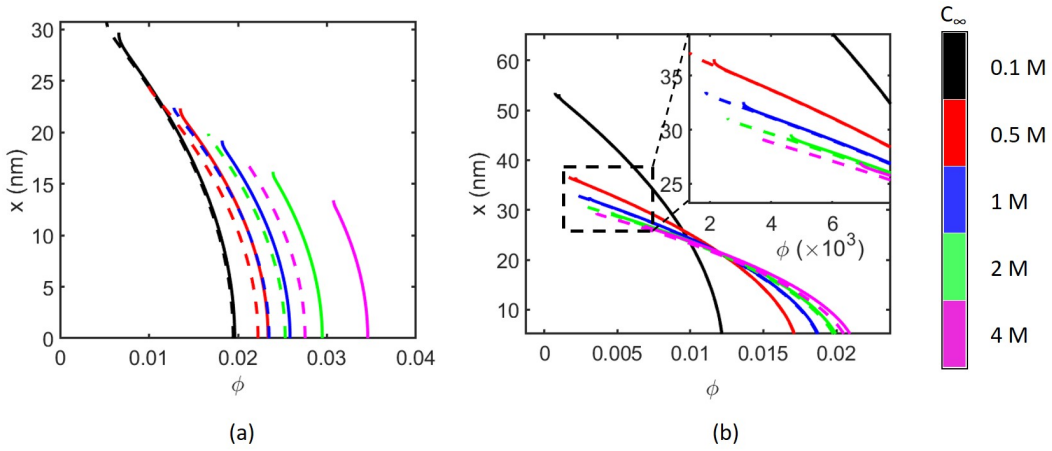

FIG. 3: Monomer density profiles for various salt concentration values for (a) $pH_\infty = 3$, and (b) $pH_\infty = 4$. Here the cases shown by solid lines (-) and dashed lines (- -) represent the cases of "IC" and "SST", respectively. Please see the caption of Fig. 2 for the definition of "IC" and "SST" cases. All other parameters are identical to those used in Fig. 2.

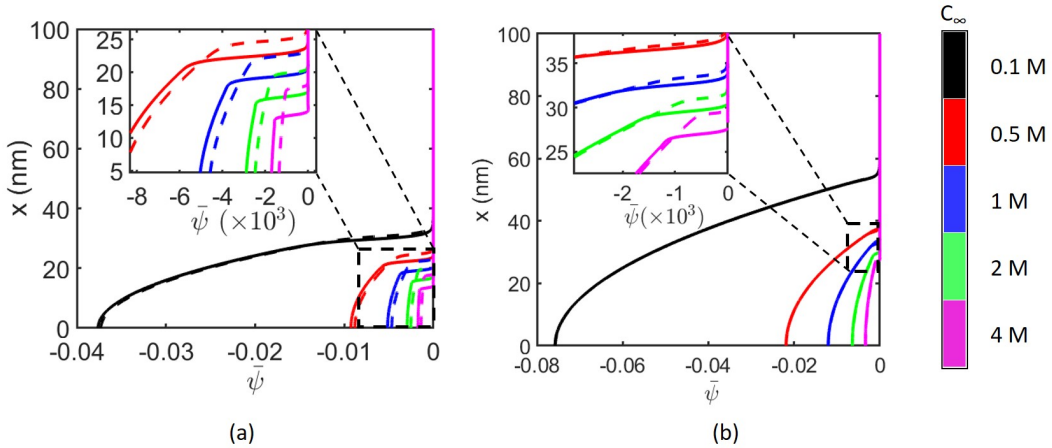

FIG. 4: Transverse variation of electrostatic EDL potential for various salt concentration values for (a) $pH_\infty = 3$, and (b) $pH_\infty = 4$. Here the cases shown by solid lines (-) and dashed lines (- -) represent the cases of "IC" and "SST", respectively. Please see the caption of Fig. 2 for the definition of "IC" and "SST" cases. All other parameters are identical to those used in Fig. 2.

In Fig. 3, we elucidate the effect of the ion-ion correlation in affecting the monomer distribution (ϕ) as a function of the salt concentration and pH_∞. Commensurate with the fact that the brush height with the consideration of the ion-ion correlation effects show the maximum difference for the cases of large salt concentration and small pH_∞ (i.e., the conditions that ensure larger number of ions), the effect of the ion-ion correlations in altering ϕ is most prominent for larger salt concentration and smaller pH_∞. Incorporating the ion-ion correlation effect yields smaller brushes (or denser brushes, i.e., brushes with lesser heights) as compared to those from the SST (without ion-ion correlation effects) [37]. A smaller brush height implies that the monomers are denser locally. This trend (showing

larger monomer concentration for the case that accounts for the ion-ion correlation effect, particularly for the condition of larger salt concentration) is readily witnessed in Figure 3. Insets to the figures have been provided to quantify the small differences in the ϕ variations for the cases of with and without the ion-ion correlation for $pH_\infty = 4$ [see Fig. 3(b)].

Fig. 4 provides the dimensionless electrostatic potential ($\bar{\psi}$) of the PE brush induced EDL. Variation of $\bar{\psi}$ for the case considering the ion-ion correlations show significant difference with respect to the case without the ion-ion correlations for pH_∞=3 and for larger salt concentrations; this difference is much smaller for smaller salt concentration and pH_∞=4. The smaller brush heights for the case considering ion-ion correlations (an effect that is augmented for large salt concentration and small pH_∞) implies that that the corresponding electrostatic potential becomes zero at shorter distances from the wall. A smaller brush height also means that the charge density of the monomer per unit volume increase, leading to a larger magnitude of $\bar{\psi}$ near the wall. For the case of pH_∞=4, the electrostatic potentials are almost indistinguishable between the cases of with and without the ion correlation effect.

B. Effect of solvent polarization

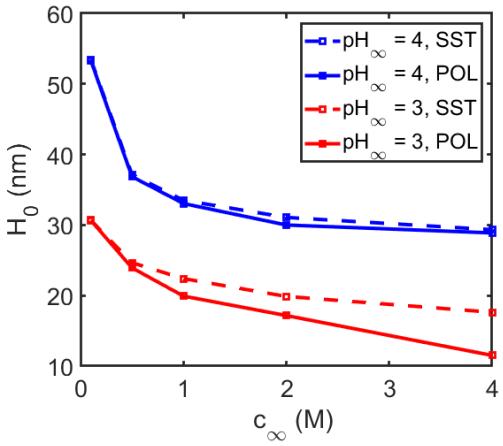

FIG. 5: Variation of the equilibrium brush height, H_0, with salt concentration for various pH_∞ values. Here, "POL" refers to the case where only the solvent polarization effect, among the different non-PB effects, has been accounted for to describe the EDL electrostatics, while the PE brushes are described using the augmented SST [37]. On the other hand, "SST" refers to the case where the EDL electrostatics is modelled using the standard PB model (i.e., we consider no non-PB term) and the PE brushes are modelled using the augmented SST [37]. We consider $p_w = 1.85\ D$, while all other parameters are identical to those used in Fig. 2.

We next consider the effect of the solvent polarization. We choose water with a dipolar moment of $p_w = 1.85\ D$ as our solvent. Polarization of the solvent molecules acts as a mechanism for the solvent molecules to realign and hence be better able to screen the PE charges. Therefore, by considering the effect of the solvent polarization one would expect a more enhanced screening effect of the EDL (in terms of the screening of the charges on the PE brushes). This is equivalent to considering a more compressed EDL, or equivalent to considering that the PE brush inter-segmental repulsions are screened over much shorter distances. Such screening would obviously imply a significant lowering of the impact of the PE brush inter-segmental electrostatic repulsion (in particular for the case of a smaller pH_∞). This, in turn, would lead to much smaller brush height as compared to the case where the solvent polarization effects have not been considered (see Fig. 5). Such solvent polarization effect induced lowering of the brush height is also enhanced for the cases of large salt concentration and low pH_∞. At a larger pH_∞, the more enhanced ionization of the PE brushes leading to a larger brush charge and hence a large PE brush inter-segmental repulsion dominates the effect of the solvent polarization, leading to a weakened effect of the solvent polarization at a larger pH_∞. At large salt concentration, where the existing EDL screening effect is already magnified, the effect of solvent polarization in further enhancing the screening effect becomes larger leading to such augmented solvent-polarization-driven reduction of the brush height.

We next plot the monomer distribution profiles in Fig. 6 for different bulk salt concentrations and pH_∞, elucidating the effect of the solvent polarization. Just like in Fig. 3, we observe an increase in the dimensionless monomer density, owing to the reduction in brush height for the case that considers the solvent polarization effect. Also, the insignificant

impact of the effect of the solvent polarization for larger pH and smaller salt concentration makes the difference in the monomer distribution (between the cases of with and without the solvent polarization) negligible.

Finally, Fig. 7 provides the normalized electrostatic potential, $\bar{\psi}$, and we observe that for pH_∞=3 and higher salt concentrations, $\bar{\psi}$ for the case considering solvent polarization effect diverges from that not considering this effect; on the other hand, for pH_∞=4, the variation of $\bar{\psi}$ for these two cases (cases with and without considering the effect of solvent polarization) are indistinguishable. Also stemming from the fact that the brush height is smaller for the cases of $pH_\infty = 3$ and large salt concentration, we find $\bar{\psi}$ becoming zero at shorter distances from the wall and showing a large magnitude at near-wall locations (where, due to the compression of the brushes, there is a larger concentration of the charged monomers).

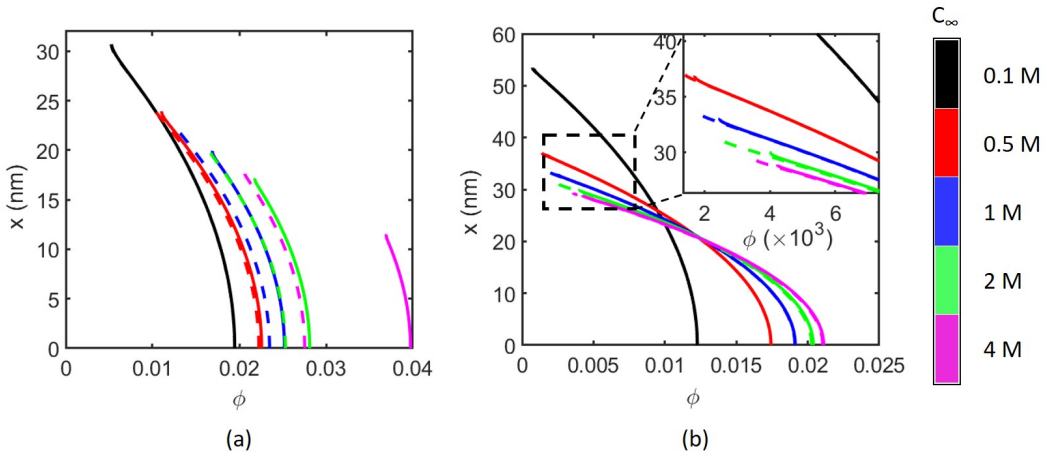

FIG. 6: Monomer density profiles for various salt concentration values for (a) $pH_\infty = 3$, and (b) $pH_\infty = 4$. Here the cases shown by solid lines (-) and dashed lines (- -) represent the cases of "POL" and "SST", respectively. Please see the caption of Fig. 5 for the definition of "POL" and "SST" cases. All other parameters are identical to those used in Fig. 5.

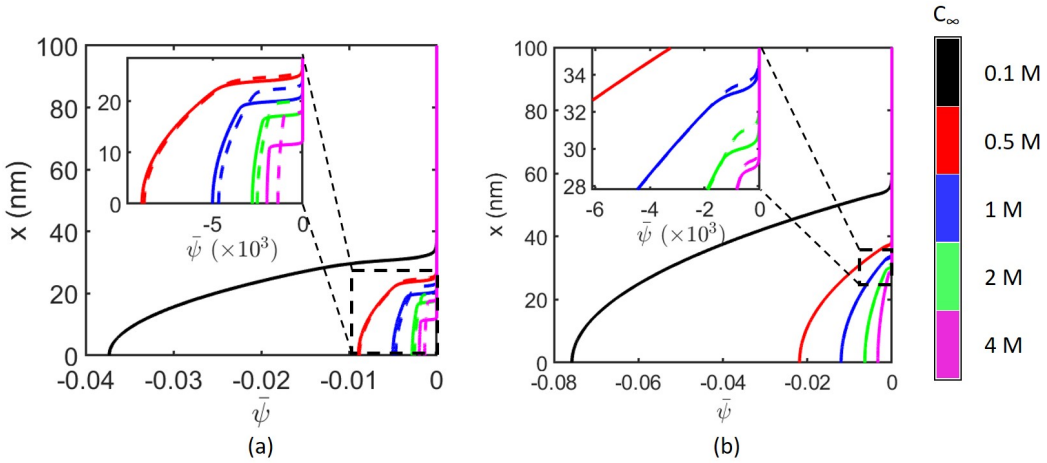

FIG. 7: Transverse variation of electrostatic EDL potential for various salt concentration values for (a) $pH_\infty = 3$, and (b) $pH_\infty = 4$. Here the cases shown by solid lines (-) and dashed lines (- -) represent the cases of "POL" and "SST", respectively. Please see the caption of Fig. 5 for the definition of "POL" and "SST" cases. All other parameters are identical to those used in Fig. 5.

C. Effect of finite sizes of the ions and dipoles

The final non-PB effect that we consider is the finite size effect for all mobile species (ions and water dipoles) in the system. For us to include the finite size effect by using the model described in the theory section of this paper,

we first need to obtain certain parameters (which are summarized in the caption of Fig. 8). We expect that the consideration of the finite size effect will enforce a lesser available volume to accommodate the counterions, which in turn decreases the entropy of the counterions; to counter this effect, the brushes stretch out more (and hence undergoes an increase in height) so that a larger space can be provided to the counterions. We indeed observe such an effect of the consideration of the finite ion and dipole sizes (see Fig. 8). Here, unlike the cases that consider either the ion-ion correlations (see Fig. 2) or solvent polarization (see Fig. 5), the difference between the cases with and without the non-PB effect (namely, the finite size effect of the ions and dipoles) is not significantly large even for larger salt concentration and small pH_∞. A possible reason for this could be that the bulk salt concentration is still not large enough to cause a massive size effect.

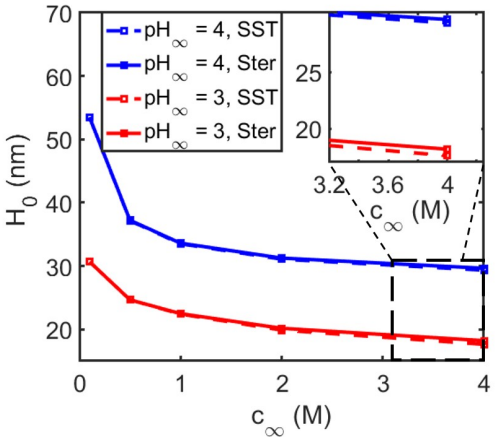

FIG. 8: Variation of equilibrium brush height, H_0, with salt concentration for various pH_∞ values. Here, "Ster" refers to the case where only the finite size effect, among the different non-PB effects, has been accounted for to describe the EDL electrostatics, while the PE brushes are described using the augmented SST [37]. On the other hand, "SST" refers to the case where the EDL electrostatics is modelled using the standard PB model (i.e., we consider no non-PB term) and the PE brushes are modelled using the augmented SST [37]. We consider $v_{H^+} = 3.4866 \times 10^{-30}$ [56] (where v_{H^+} denotes the volume of H^+ ion, which is the smallest species in our lattice model and occupies just one lattice site), $\xi_+ = v_+/v_{H^+} = 39.3674$, $\xi_- = v_-/v_{H^+} = 26.3731$, $\xi_w = v_w/v_{H^+} = 3.1779$, $\xi_{H^+} = 1$, and $\xi_{OH^-} = v_{OH^-}/v_{H^+} = 3.7143$ [55, 56]. All other parameters are identical to those used in Fig. 2.

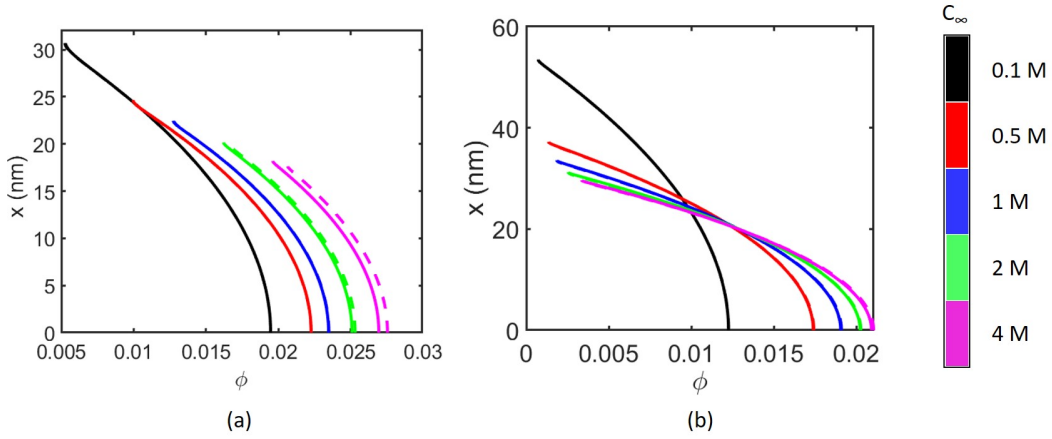

FIG. 9: Monomer density profiles for various salt concentration values for (a) $pH_\infty = 3$, and (b) $pH_\infty = 4$. Here the cases shown by solid lines (-) and dashed lines (- -) represent the cases of "Ster" and "SST", respectively. Please see the caption of Fig. 8 for the definition of "Ster" and "SST" cases. All other parameters are identical to those used in Fig. 8.

Figures 9 and 10 show respectively the dimensionless monomer density and the electrostatic potential ($\bar{\psi}$), elucidating the effect of considering the finite size effect. The monomer distribution has smaller magnitude, since the brush heights were slightly larger, for the case with finite ion sizes. Of course, only for the cases of largest bulk salt

concentration (2 M, 4 M) and $pH_\infty = 3$, we see some difference in the monomer distribution between the cases of with and without the finite size effect. For other salt concentration and pH_∞ combinations, this difference between the cases of with and without the finite size effect becomes insignificant. On the other hand, the larger brush size and the weaker monomer distribution implies that for the case that considers the finite size effect, the electrostatic potential goes to zero at distances further away from the wall and has a weaker magnitude at near-wall locations (see Fig. 10).

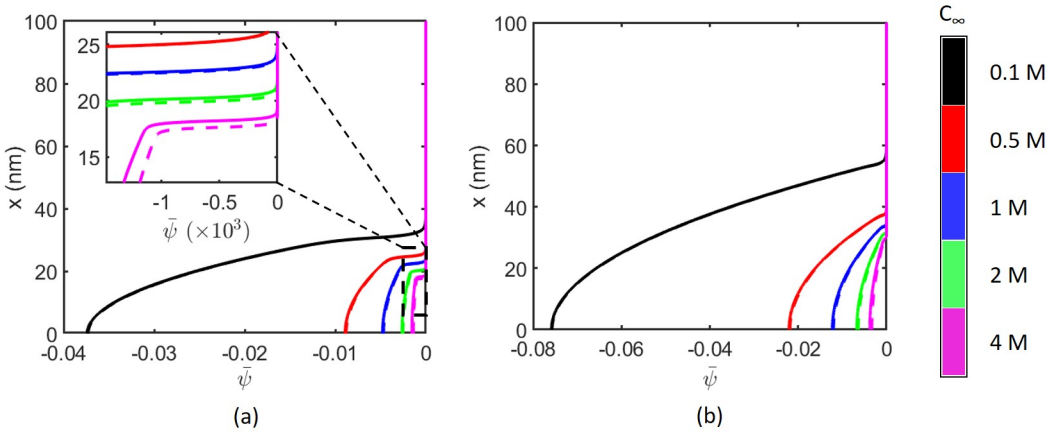

FIG. 10: Transverse variation of electrostatic EDL potential for various salt concentration values for (a) $pH_\infty = 3$, and (b) $pH_\infty = 4$. Here the cases shown by solid lines (-) and dashed lines (- -) represent the cases of "Ster" and "SST", respectively. Please see the caption of Fig. 8 for the definition of "Ster" and "SST" cases. All other parameters are identical to those used in Fig. 8.

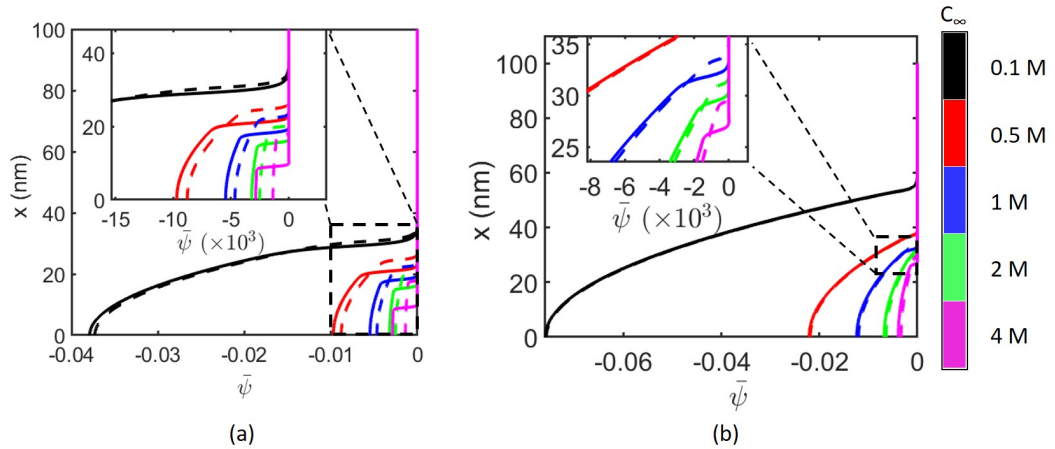

FIG. 11: Transverse variation of electrostatic EDL potential for various salt concentration values for (a) $pH_\infty = 3$, and (b) $pH_\infty = 4$. Here the cases shown by solid lines (-) and dashed lines (- -) represent the cases of "MSST" and "SST", respectively. Please see the caption of Fig. 12 for the definition of "MSST" and "SST" cases. All other parameters are identical to those used in Fig. 12.

D. Effect of all the different non-PB contributions considered simultanoeusly

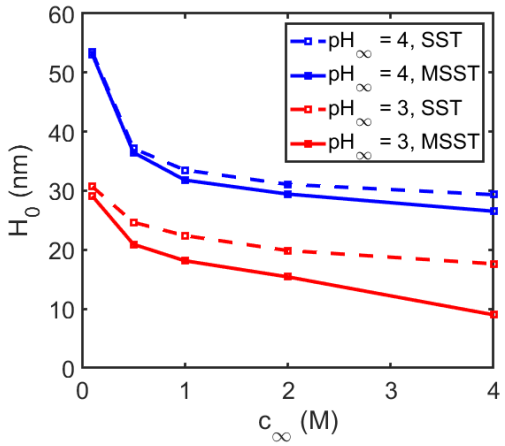

FIG. 12: Variation of equilibrium brush height, H_0, with salt concentration for various pH_∞ values. Here, "MSST" refers to the case of modified augmented SST: for this case all the three different non-PB effects (ion-ion correlation, solvent polarization, and finite ion and dipole size) have been considered simultaneously to describe the EDL electrostatics, while the PE brushes are described using the augmented SST [37]. On the other hand, "SST" refers to the case where the EDL electrostatics is modelled using the standard PB model (i.e., we consider no non-PB term) and the PE brushes are modelled using the augmented SST [37]. Here we use $l_c = 0.3\ nm$, $p_w = 1.85\ D$, $v_{H^+} = 3.4866 \times 10^{-30}$ [56], $\xi_+ = v_+/v_{H^+} = 39.3674$, $\xi_- = v_-/v_{H^+} = 26.3731$, $\xi_w = v_w/v_{H^+} = 3.1779$, $\xi_{H^+} = 1$, and $\xi_{OH^-} = v_{OH^-}/v_{H^+} = 3.7143$ [55, 56]. All other parameters are identical to that used in Fig. 2.

Finally, we provide the results showcasing the impact of all the three different non-PB effects (ion-ion correlation, solvent polarization, and finite ion and dipole size) considered simultaneously on the brush configuration (quantified through the variation of the brush height and the monomer distribution) and the brush-induced EDL (quantified through the variation of the EDL electrostatic potential). We denote this case (the one that considers all the three different non-PB effects) as the modified augmented SST (or MSST). The equilibrium brush height shows a net reduction due to the consideration of the non-PB effects: both the ion-ion correlation as well as the solvent polarizability effect cause a significant reduction in the brush height and dominate the effect of the consideration of finite sizes (that only causes a weak increase in the brush height). Commensurate with the variation where the individual effects were considered in isolation, we find that the reduction in the brush height is maximum for the cases of larger salt concentration and smaller pH_∞. This in turn translates to a larger magnitude of dimensionless monomer densities (see Fig. 13) and an electrostatic potential distribution (see Fig. 11) that has a large magnitude at near-wall locations and becomes zero at shorter distances from the wall. Also, very much like the case of the height variation, these distinct trends in the monomer and electrostatic potential distribution become observable for the cases of large salt concentration and small pH_∞.

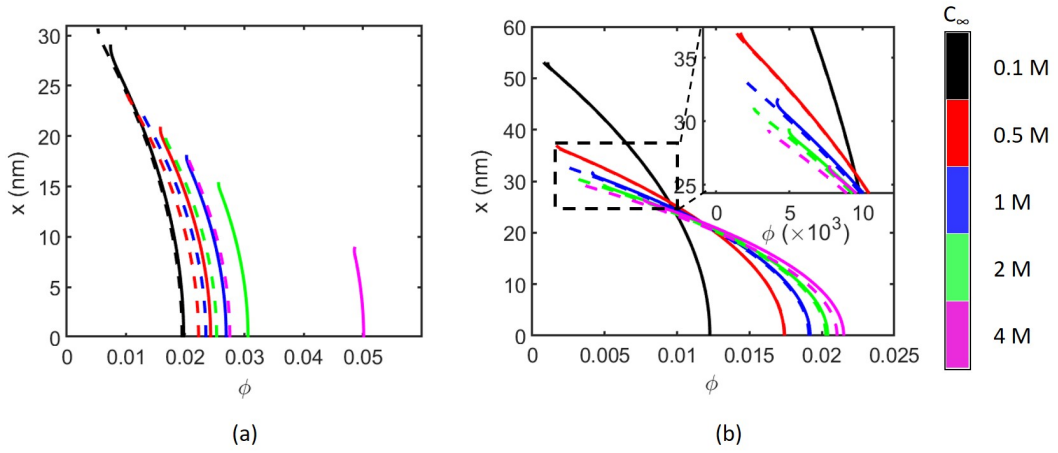

FIG. 13: Monomer density profiles for various salt concentration values for (a) $pH_\infty = 3$, and (b) $pH_\infty = 4$. Here the cases shown by solid lines (-) and dashed lines (- -) represent the cases of "MSST" and "SST", respectively. Please see the caption of Fig. 12 for the definition of "MSST" and "SST" cases. All other parameters are identical to those used in Fig. 12.

IV. COMPARISON WITH ALL-ATOM MD SIMULATION RESULTS

In this section, we compare the results (the brush height) from our present theoretical model with those obtained from our recent all-atom molecular dynamics (MD) simulation study on PE brushes [44]. The system probed by the all-atom simulations consist of fully ionized Polyacrylic acid (PAA) brushes neutralized by counterions. The MD simulations probed different values of chain lengths (quantified by the number of backbone Carbon atoms) and grafting densities (quantified by the lateral separation between adjacent chains). We provide results for the brush height predicted from our present theory and that obtained from the atomistic simulations (see Table 1) and we observe a most outstanding match (discussed in more details later).

In order to make a one-to-one comparison of our theoretical results with the simulations, we make a few assumptions. Firstly, we consider each C-C bond in the PAA backbone (along with the attached pendant groups) (as represented in the all-atom MD model) as one Kuhn segment in the present theoretical model. This gives us a Kuhn length of $a = 1.53$Å and the number of Kuhn segments equal to the number of C-C bonds (along the backbone of the individual PAA chains) for using in our theoretical model. For example, a chain having 29 backbone Carbon atoms in the MD simulation will contain 28 backbone C-C bonds and thus 28 Kuhn segments. Of course, with such considerations we neglect the effect of the strong angular and torsional constraints along the PAA backbone. Moreover, since fully ionized PAA chains contain a carboxylate group on every alternate backbone carbon atom, we set the density of polyelectrolyte chargeable sites to $\gamma = 0.5/a^3$.

Our second assumption relates to the quantification of an equivalent bulk salt concentration for the MD simulations. The simulations have some fundamental differences from the theoretical model as the simulations consider the effect of the counterions explicitly. In fact, the cation concentration within the brushes in our MD simulations was primarily due to the presence of the explicit counterions. We had added 0.1 M NaCl salt in the simulation box as well (for our MD simulation study [44]), but its concentration within the brushes was negligible in comparison to the counterions. On the other hand, our theoretical model involves the effects of a bulk salt concentration but does not consider the counterions (in the vicinity of the PE brushes) separately. Thus, in order to make an appropriate comparison between the two systems, we have ensured that the cation (or counterion) concentration within the brushes is equal for the two cases (i.e, the case studied by the MD simulations and the present case). This was achieved by varying the bulk salt concentration in our theoretical model (for each value of chain length and grafting density) until we obtained an average cation concentration within the brushes (for our theoretical model) that is nearly identical to the counterion concentration within the brushes obtained from the simulations. Of course, the anion concentration within the brushes is negligible due to the presence of negative charges on the PE functional groups and the fact that the brushes are extremely densely grafted and hence can be ignored. The final bulk salt concentration values used in the theoretical model as well as the average cation (counterion) concentrations within the brushes for the present theory (MD simulations of Ref. [44]) are provided in Table 1 and as one could see, we work with almost identical concentration values (for the two cases).

Finally, in order to enforce complete ionization of the PE functional groups in our model, we set $pH_\infty \gg pKa$. This was done to be consistent with the MD simulations that considered fully ionized PAA chains.

From Table 1, we observe an excellent match between the brush heights predicted by our MSST model and the all-atom MD simulations. In fact, the brush heights differ by less than 5% for all the different combinations of parameters that were considered. This level of agreement with the MD simulation results is remarkable, considering the sophistication involved in such atomistic simulations that considered an all-atom framework where each atom of the brushes, water and the mobile ions were modelled explicitly. This allows the simulations to attain levels of accuracy that are beyond the capabilities of any mean field continuum model. Despite that, our theoretical results are in outstanding agreement with the MD simulation results. This not only validates our model but also testifies its potential in capturing non-PB effects to an extent that is unprecedented in the continuum modelling of PE brushes.

Number of carbon atoms (**N**)	Grafting Density ($\sigma_{\mathbf{g}}$) ($1/\sigma^2$)	Bulk salt concentration used for the MSST model [$\mathbf{c}_\infty$ (M)]	Average counterion concentration within PE brushes for Ref. [44] (M)	Average cation concentration within PE brushes for the MSST model (M)	Brush Height (Å) obtained in Ref. [44]	Brush Height (Å) obtained using the MSST model
29	0.05	0.1	3.38	3.43	25.56	24.92
29	0.1	0.6	6.04	6.00	28.99	29.50
49	0.05	0.3	3.47	3.46	44.25	45.40
49	0.1	1.25	6.19	6.21	50.43	50.91
69	0.05	0.5	3.57	3.62	61.98	62.86
69	0.1	1.5	6.32	6.30	70.53	72.86

TABLE I: Comparison of brush heights obtained from the MSST model developed in this paper and all-atom MD simulations of Ref. [44] for various values of the number of carbon atoms (N) and grafting density (in units of $1/\sigma^2$, where $\sigma = 3.5$Å is the Lennard Jones size parameter). The values of bulk salt concentration (c_∞ in M) used in MSST model, the equivalent average cation concentration within the brushes for the MSST model, and the average counterion concentration for the MD simulations are also provided. Please note for a given N and σ_g value, we consider such a value of the bulk salt concentration that yields nearly identical values of cation concentration and counterion concentration for the MSST model and the MD simulations, respectively. Only under such circumstances, we could compare that height values obtained from the present MSST model and the all-atom MD simulations. Other parameters used in the MSST model are as follow: Kuhn length, a, of 1 C-C bond length equivalent to 1.53Åand the density of chargeable sites (γ) equal to $0.5/a^3$.

V. CONCLUSIONS

In this paper, we develop for the first time a detailed theoretical model for describing the thermodynamics, configurations, and electrostatics of the pH-responsive, PE brushes in presence of a large salt concentration. The theory combines our recently developed augmented SST [37] for describing the PE brushes with the model proposed by McEldrew *et al* [42] that accounts for the appropriate non-PB effects [non-mean-field electrostatic ion-ion correlations, solvent polarization, and the finite size (ion and water dipole) effects] for describing the free energy of the large-concentration electrolytes. Our results point out that these different non-PB effects compete with each other and eventually ensure, in a scenario where the ion-ion correlation and the solvent polarization effects outweigh the influence of the finite size effect, the PE brush height decreases, thereby increasing the monomer density and inducing an EDL electrostatic potential distribution that has a larger magnitude at near-wall locations and becomes zero at shorter distances away from the wall. Furthermore, we also discover that the influence of the non-PB effects are maximum at large salt concentrations and small bulk pH. Finally, we are able to validate our model by comparing its findings with those of our recent all-atom MD simulation study.

In the end, we would like to add a few points regarding the limitations of the present theory. Here we account for the ion-ion correlations only between the mobile ions (i.e., the EDL ions). Such a consideration overlooks the effect of the possible correlation between the static charged functional groups of the PE brushes and the EDL ions (especially the counterions). To the best of our knowledge, no theory exist that accounts for such a correlation; however, it is definitely worthwhile to investigate in future if such a correlation between the charges of the PE brushes and the counterions can be of any consequence in the thermodynamics, configuration, and electrostatics of densely grafted brushes in large salt concentrations. Secondly, we do not consider the ion-partitioning effect, which stems from a possible mismatch between the solvent permittivities inside and outside the PE brushes and have been known to have some effect on the overall electrostatics of the brush-induced EDL [57].

Acknowledgement: This work has been supported by the Department of Energy Office of Science grant DE-SC0017741.

Appendix A: Detailed derivation of eq.(9)

Eq.(5) expresses δF_e in terms of $\delta \mathbf{D}$. Using eqs.(6,7,8), we can write:

$$\delta \boldsymbol{D} = \frac{\delta P_{pol}}{\delta \boldsymbol{E}} \delta \boldsymbol{E} + \varepsilon_0 \varepsilon_r \delta \boldsymbol{E} - \varepsilon_0 \varepsilon_r l_c^2 \delta(\nabla \cdot \nabla) \boldsymbol{E}. \tag{A1}$$

Using eq.(A1) along with the vector identity $\nabla \cdot \nabla \boldsymbol{E} = \nabla(\nabla \cdot \boldsymbol{E}) - \nabla \times (\nabla \times \boldsymbol{E}) = \nabla(\nabla \cdot \boldsymbol{E})$ (since $\nabla \times \boldsymbol{E} = -\nabla \times \nabla \psi = 0$), we can re-write eq.(5) as:

$$\delta F_e = \int_V \left[\frac{\delta P_{pol}}{\delta \boldsymbol{E}} \boldsymbol{E} \cdot \delta \boldsymbol{E} + \varepsilon_0 \varepsilon_r \boldsymbol{E} \cdot \delta \boldsymbol{E} - \varepsilon_0 \varepsilon_r l_c^2 \boldsymbol{E} \cdot \nabla \delta(\nabla \cdot \boldsymbol{E}) \right] dV. \tag{A2}$$

The vector identity, $\boldsymbol{E} \cdot \nabla \delta(\nabla \cdot \boldsymbol{E}) = \nabla \cdot (\boldsymbol{E} \delta(\nabla \cdot \boldsymbol{E})) - \nabla \cdot \boldsymbol{E} \delta(\nabla \cdot \boldsymbol{E})$, can then be used, where divergence theorem can be employed so that the first term on the right hand side of the equation vanishes because of zero electric field at the substrate and at infinity. Therefore, eq.(A2) reduces to:

$$\delta F_e = \int_V \left[\frac{\delta P_{pol}}{\delta \boldsymbol{E}} \boldsymbol{E} \cdot \delta \boldsymbol{E} + \varepsilon_0 \varepsilon_r \boldsymbol{E} \cdot \delta \boldsymbol{E} + \varepsilon_0 \varepsilon_r l_c^2 \nabla \cdot \boldsymbol{E} \delta(\nabla \cdot \boldsymbol{E}) \right] dV. \tag{A3}$$

We next take the variational integral of δF_e from 0 to F_e and enforce the condition, $\nabla \cdot \boldsymbol{D} = \rho_e$ [where $\rho = e(n_+ - n_- + n_{H^+} - n_{OH^-})$ is the volume charge density of mobile ions] using a Lagrange multiplier λ, to yield:

$$F_e = \int_V \left[\frac{n_w}{\beta} \left(\beta p_w \nabla \psi \mathcal{L}(\beta p_w \nabla \psi) - \ln \left(\frac{sinh(\beta p_w \nabla \psi)}{\beta p_w \nabla \psi} \right) \right) + \frac{\varepsilon_0 \varepsilon_r}{2} \left(|\nabla \psi|^2 + l_c^2 |\nabla^2 \psi|^2 \right) + \lambda(\rho_e - \nabla \cdot \boldsymbol{D}) \right] dV. \tag{A4}$$

Substituting eq.(6) in eq.(A4) and using the Frechet functional derivative, $\frac{\delta F_e}{\delta \psi} = \lim_{\epsilon \to 0} \frac{F_e(\psi + \epsilon \psi_0 \delta_\epsilon) - F_e(\psi)}{\epsilon \psi_0} = 0$, we obtain $\lambda = \psi$; hence eq.(A4) reduces to eq.(9).

Appendix B: Detailed derivation of eq.(11)

We start with eq.(10) and apply the conditions $Q(\chi_j) = \omega_j e^{-\beta \epsilon_j \chi_j}$, $E_j = \epsilon_j \chi_j$, $\omega_j = \frac{N_t!}{\chi_j!(N_t - \chi_j)!}$, $\xi_j = v_j \ / v_{H^+}$, and $\tilde{\mu}_j = \mu_j - \epsilon_j$ to reduce eq.(10) to:

$$\Xi = \sum_{\chi_w=0}^{N_t/\xi_w} \omega_w e^{\beta \tilde{\mu}_w \chi_w} \cdot \sum_{\chi_-=0}^{(N_t - \xi_w \chi_w)/\xi_-} \omega_- e^{\beta \tilde{\mu}_- \chi_-} \cdot \sum_{\chi_+=0}^{(N_t - \chi_w - \xi_- \chi_-)/\xi_+} \omega_+ e^{\beta \tilde{\mu}_+ \chi_+} \cdot \sum_{\chi_{H^+}=0}^{(N_t - \chi_w - \xi_- \chi_- - \xi_+ \chi_+)/\xi_{H^+}} \omega_{H^+} e^{\beta \tilde{\mu}_{H^+} \chi_{H^+}} \cdot \sum_{\chi_{OH^-}=0}^{(N_t - \chi_w - \xi_- \chi_- - \xi_+ \chi_+ - \xi_{H^+})/\xi_{OH^-}} \omega_{OH^-} e^{\beta \tilde{\mu}_{OH^-} \chi_{OH^-}}. \tag{B1}$$

The summations in the partition function can then be evaluated using the binomial theorem, assuming a progressive filling of the lattice sites with each species. Accordingly, eq.(B1) reduces to

$$\Xi = \left[\left(\left(\left(\left\{ 1 + e^{\beta \tilde{\mu}_{OH^-}} \right\}^{\xi_{H^+}/\xi_{OH^-}} + e^{\beta \tilde{\mu}_{H^+}} \right)^{\xi_+/\xi_{H^+}} + e^{\beta \tilde{\mu}_+} \right)^{\xi_-/\xi_+} + e^{\beta \tilde{\mu}_-} \right)^{\xi_w/\xi_-} + e^{\beta \tilde{\mu}_w} \right]^{N_t/\xi_w}. \tag{B2}$$

Given that $PV_L = k_B T ln \Xi$, where $V_L = N_t v_{H^+}$, we can finally write from eq.(B2)

$$P = \frac{k_B T}{v_{H^+}} ln \left[\left(\left(\left(\left\{ 1 + e^{\beta \tilde{\mu}_{OH^-}} \right\}^{\xi_{H^+}/\xi_{OH^-}} + e^{\beta \tilde{\mu}_{H^+}} \right)^{\xi_+/\xi_{H^+}} + e^{\beta \tilde{\mu}_+} \right)^{\xi_-/\xi_+} + e^{\beta \tilde{\mu}_-} \right)^{\xi_w/\xi_-} + e^{\beta \tilde{\mu}_w} \right]^{1/\xi_w}, \tag{B3}$$

or, by taking constants out of $\tilde{\mu}_j$, we can write,

$$P = \frac{k_B T}{v_{H^+}} ln \left[\left(\left(\left(\left\{ 1 + \xi_{OH^-} e^{\beta \tilde{\mu}_{OH^-}} \right\}^{\xi_{H^+}/\xi_{OH^-}} + \xi_{H^+} e^{\beta \tilde{\mu}_{H^+}} \right)^{\xi_+/\xi_{H^+}} + \xi_+ e^{\beta \tilde{\mu}_+} \right)^{\xi_-/\xi_+} + \xi_- e^{\beta \tilde{\mu}_-} \right)^{\xi_w/\xi_-} + \xi_w e^{\beta \tilde{\mu}_w} \right]^{1/\xi_w}, \tag{B4}$$

which is eq.(11).

Appendix C: Detailed minimization procedure for the terms of f_{brush}

We first consider the variational minimization of the terms of f_{brush} (i.e., perform the variational minimization w.r.t $E(x,x')$, $g(x')$, and n_{A^-}), yielding:

$$\begin{aligned}
\delta \int_V f_{brush}\, dV = {} & \frac{3k_BT}{2pa^2} \Big[\int_0^H g(x')dx' \int_0^{x'} \delta E(x,x')dx + \int_0^H \delta g(x')dx' \int_0^{x'} E(x,x')dx \Big] + \lambda_1 \frac{k_BT\sigma}{a^3} \int_0^H \delta\phi(x)dx \\
& - k_BT \int_0^H \lambda_2(x')dx' \int_0^{x'} \frac{\delta E(x,x')}{E^2(x,x')}dx + \frac{k_BT\sigma}{a^3} \int_0^H \Big(\frac{\delta f_{conc}}{\delta\phi} \Big) \delta\phi dx \\
& - \sigma \int_0^H \Big[e\phi n_{A^-} \delta\psi + e\phi\psi\delta n_{A^-} + e\psi n_{A^-} \delta\phi \Big] dx \\
& + \frac{k_BT\sigma}{a^3} \int_0^H \delta\phi \left[\Big(1 - \frac{n_{A^-}}{\gamma}\Big) ln\Big(1 - \frac{n_{A^-}}{\gamma}\Big) + \frac{n_{A^-}}{\gamma} ln\Big(\frac{n_{A^-}}{\gamma}\Big) + \frac{n_{A^-}}{\gamma} ln\Big(\frac{n_{H^+,\infty}}{K'_a}\Big) \right] dx \\
& + \frac{k_BT\sigma}{a^3} \int_0^H \delta n_{A^-} \phi \left[-\frac{1}{\gamma} ln\Big(1 - \frac{n_{A^-}}{\gamma}\Big) + \frac{1}{\gamma} ln\Big(\frac{n_{A^-}}{\gamma}\Big) + \frac{1}{\gamma} ln\Big(\frac{n_{H^+,\infty}}{K'_a}\Big) \right] dx,
\end{aligned} \tag{C1}$$

where the variational of ϕ is expressed as:

$$\delta\phi(x) = \frac{a^3}{\sigma} \int_x^H \Big[\frac{\delta g(x')}{E(x,x')} - \frac{g(x')\delta E(x,x')}{E^2(x,x')} \Big] dx'. \tag{C2}$$

Using eq.(C2), we can re-write eq.(C1) as:

$$\begin{aligned}
\delta \int_V f_{brush}\, dV = {} & k_BT \int_0^H dx' \int_0^{x'} \delta E(x,x') \left[\frac{3g(x')}{2pa^2} - \frac{\lambda_2(x')}{E^2(x,x')} - \left(\frac{\delta f_{conc}}{\delta\phi} + \lambda_1 - \frac{ea^3\psi}{k_BT} n_{A^-} + \Big(1 - \frac{n_{A^-}}{\gamma}\Big) ln\Big(1 - \frac{n_{A^-}}{\gamma}\Big) \right. \right. \\
& \left. \left. + \frac{n_{A^-}}{\gamma} ln\Big(\frac{n_{A^-}}{\gamma}\Big) + \frac{n_{A^-}}{\gamma} ln\Big(\frac{n_{H^+,\infty}}{K'_a}\Big) \right) \frac{g(x')}{E^2(x,x')} \right] dx \\
& + k_BT \int_0^H dx' \delta g(x') \int_0^{x'} \left[\frac{3E(x,x')}{2pa^2} + \left(\frac{\delta f_{conc}}{\delta\phi} + \lambda_1 - \frac{ea^3\psi}{k_BT} n_{A^-} + \Big(1 - \frac{n_{A^-}}{\gamma}\Big) ln\Big(1 - \frac{n_{A^-}}{\gamma}\Big) \right. \right. \\
& \left. \left. + \frac{n_{A^-}}{\gamma} ln\Big(\frac{n_{A^-}}{\gamma}\Big) + \frac{n_{A^-}}{\gamma} ln\Big(\frac{n_{H^+,\infty}}{K'_a}\Big) \right) \frac{1}{E(x,x')} \right] dx \\
& + \frac{k_BT\sigma}{\gamma a^3} \int_0^H \delta n_{A^-} \phi \left[-\gamma a^3 \frac{e\psi}{k_BT} - ln\Big(1 - \frac{n_{A^-}}{\gamma}\Big) + ln\Big(\frac{n_{A^-}}{\gamma}\Big) + ln\Big(\frac{n_{H^+,\infty}}{K'_a}\Big) \right] dx.
\end{aligned} \tag{C3}$$

From the fact that $\delta \int_V f_{brush}\, dV = 0$ (dictated by the equilibrium condition) and that $\delta E(x,x') \neq 0$, $\delta g \neq 0$ and $\delta n_{A^-} \neq 0$, we arrive at the following equations that govern the brush structure:

$$\begin{aligned}
& \frac{3g(x')}{2a^2} - \frac{\lambda_2(x')}{E^2(x,x')} - \left(\frac{\delta f_{conc}}{\delta\phi} + \lambda_1 - \frac{ea^3\psi}{k_BT} n_{A^-} + \Big(1 - \frac{n_{A^-}}{\gamma}\Big) ln\Big(1 - \frac{n_{A^-}}{\gamma}\Big) \right. \\
& \left. + \frac{n_{A^-}}{\gamma} ln\Big(\frac{n_{A^-}}{\gamma}\Big) + \frac{n_{A^-}}{\gamma} ln\Big(\frac{n_{H^+,\infty}}{K'_a}\Big) \right) \frac{g(x')}{E^2(x,x')} = 0,
\end{aligned} \tag{C4}$$

$$\int_0^{x'}\Bigg[\frac{3E(x,x')}{2a^2}+\Bigg(\frac{\delta f_{conc}}{\delta\phi}+\lambda_1-\frac{ea^3\psi}{k_BT}n_{A^-}+\Big(1-\frac{n_{A^-}}{\gamma}\Big)ln\Big(1-\frac{n_{A^-}}{\gamma}\Big)+\frac{n_{A^-}}{\gamma}ln\Big(\frac{n_{A^-}}{\gamma}\Big) + \frac{n_{A^-}}{\gamma}ln\Big(\frac{n_{H^+,\infty}}{K_a'}\Big)\Bigg)\frac{1}{E(x,x')}\Bigg]dx=0, \tag{C5}$$

$$\begin{aligned} &-\gamma a^3\frac{e\psi}{k_BT}-ln\Big(1-\frac{n_{A^-}}{\gamma}\Big)+ln\Big(\frac{n_{A^-}}{\gamma}\Big)+ln\Big(\frac{n_{H^+,\infty}}{K_a'}\Big)=0 \\ &\implies n_{A^-}=\frac{K_a'\gamma}{K_a'+n_{H^+,\infty}\exp\big(-\gamma a^3\frac{e\psi}{k_BT}\big)}. \end{aligned} \tag{C6}$$

Eq.(C5) is eq.(23) and eq.(C6) is eq.(24).

Subsequently, rearranging the terms in eq.(C4), we obtain:

$$E(x,x')=\sqrt{U_1(x')-U_2(x)}, \tag{C7}$$

with

$$U_1(x')=\frac{2a^2}{3}\frac{\lambda_2(x')}{g(x')}, \tag{C8}$$

$$U_2(x)=\frac{2a^2}{3}\Bigg(-\frac{\delta f_{conc}}{\delta\phi}-\lambda_1+\frac{ea^3\psi}{k_BT}n_{A^-}-\Big(1-\frac{n_{A^-}}{\gamma}\Big)ln\Big(1-\frac{n_{A^-}}{\gamma}\Big)-\frac{n_{A^-}}{\gamma}ln\Big(\frac{n_{A^-}}{\gamma}\Big)-\frac{n_{A^-}}{\gamma}ln\Big(\frac{n_{H^+,\infty}}{K_a'}\Big)\Bigg). \tag{C9}$$

For any PE chain, the stretching/extension at the chain end is $E(x',x')=0$, and the chain end location (x') itself is a continuous function with values between 0 and H. Therefore, $U_1(x')=U_2(x')=U(x')=U(x)$. Hence,

$$E(x,x')=\sqrt{U(x')-U(x)}. \tag{C10}$$

Using the normalization condition of eq.(19) to the above equation, one subsequently arrives at an integral equation for $U(x')$ which is satisfied if:

$$U(x)=\frac{\pi^2x^2}{4N^2}, \tag{C11}$$

which in turn leads to:

$$E(x,x')=\frac{\pi}{2N}\sqrt{x'^2-x^2}. \tag{C12}$$

Eq.(C12) is eq.(22).
Eq.(23) gives us an additional integral equation, given below, that is to be satisfied by this choice of $U(x)$.

$$\int_0^{x'}\Big[E(x,x')-\frac{U(x)}{E(x,x')}\Big]dx=0. \tag{C13}$$

We next use the following dependence (virial expansion) of f_{conc} (contribution to the free energy due to excluded volume interaction) on ϕ:

$$f_{conc}[\phi(x)]\approx\nu_0\phi^2+\omega_0\phi^3+\dots, \tag{C14}$$

where ν_0 and ω_0 are called virial coefficients. Using eq.(C14) to obtain $\frac{\delta f_{conc}}{\delta\phi}$ in eq.(C9) and using the condition $U_2(x')=U(x)$ and eq.(C11), we finally obtain from eq.(C9) the following equation connecting the monomer distribu-

tion ϕ to the electrostatic potential ψ:

$$\begin{aligned}\phi(x) =&\frac{\nu}{3\omega}\Bigg[\Bigg\{1+\kappa^2\Bigg(\lambda-x^2+\alpha\frac{K_a'\gamma}{K_a'+n_{H^+,\infty}\exp\big(-\gamma a^3\frac{e\psi}{k_BT}\big)}\psi\\&-\rho\Big(1-\frac{K_a'}{K_a'+n_{H^+,\infty}\exp\big(-\gamma a^3\frac{e\psi}{k_BT}\big)}\Big)ln\Big(1-\frac{K_a'}{K_a'+n_{H^+,\infty}\exp\big(-\gamma a^3\frac{e\psi}{k_BT}\big)}\Big)\\&-\rho\frac{K_a'}{K_a'+n_{H^+,\infty}\exp\big(-\gamma a^3\frac{e\psi}{k_BT}\big)}ln\Big(\frac{K_a'}{K_a'+n_{H^+,\infty}\exp\big(-\gamma a^3\frac{e\psi}{k_BT}\big)}\Big)\\&-\rho\frac{K_a'}{K_a'+n_{H^+,\infty}\exp\big(-\gamma a^3\frac{e\psi}{k_BT}\big)}ln\Big(\frac{n_{H^+,\infty}}{K_a'}\Big)\Bigg)\Bigg\}^{1/2}-1\Bigg].\end{aligned}\tag{C15}$$

Eq.(C15) is the same as eq.(25) and the different terms of eq.(25) are provided below eq.(25).

[1] G. W. de Groot, M. G. Santonicola, K. Sugihara, T. Zambelli, E. Reimhult, J. Voros and G. J. Vancso, *ACS Appl. Mater. Interface.*, 2013, **5**, 1400–1407.
[2] B. Yameen, M. Ali, R. Neumann, W. Ensinger, W. Knoll and O. Azzaroni, *J. Am. Chem. Soc.*, 2009, **131**, 2070–2071.
[3] M. Ali, B. Yameen, R. Neumann, W. Ensinger, W. Knoll and O. Azzaroni, *J. Am. Chem. Soc.*, 2008, **130**, 16351–16357.
[4] M. Ali, B. Schiedt, R. Neumann and W. Ensinger, *Macromol. Biosci.*, 2010, **10**, 28–32.
[5] S. Umehara, M. Karhanek, R. W. Davis and N. Pourmand, *Proc. Natl. Acad. Sci.*, 2009, **106**, 4611–4616.
[6] M. Ali, B. Yameen, J. Cervera, P. Ramirez, R. Neumann, W. Ensinger, W. Knoll and O. Azzaroni, *J. Am. Chem. Soc.*, 2010, **132**, 8338–8348.
[7] M. Ali, P. Ramirez, S. Mafe, R. Neumann and W. Ensinger, *ACS Nano* **2009**, 21, 9873–9878.
[8] B. Jaquet, D. Wei, B. Reck, F. Reinhold, X. Zhang, H. Wu and M. Morbidelli, *Colloid and Polymer Science*, 2013, **291**, 1659-1667.
[9] N. Saleh, T. Sarbu, K. Sirk, G. V. Lowry, K. Matyjaszewski and R. D. Tilton, *Langmuir*, 2005, **3**, 603–608.
[10] G. Liu, M. Cai, X. Wang, F. Zhou and W. Liu, *ACS Appl. Mater. Interface*, 2014, **6**, 11625–11632.
[11] A. K. Bajpai, S. K. Shukla, S. Bhanu, and S. Kankane, *Prog. Polym. Sci.*, 2008, **33**, 1088–1118.
[12] P. A. Pincus, *Macromolecules*, 1991, **24**, 2912–2919.
[13] R. Ross and P. A. Pincus, *Macromolecules*, 1992, **25**, 2177–2183.
[14] O. V. Borisov, T. M. Birshtein and E. B. Zhulina, *J. Phys. II*, 1991, **1**, 521–526.
[15] J. Wittmer and J. F. Joanny, *Macromolecules*, 1993, **26**, 2691–2697.
[16] O. V. Borisov, E. B. Zhulina and T. M. Birshtein, *Macromolecules*, 1994, **27**, 4795–4803.
[17] E. B. Zhulina, T. M. Birshtein and O. V. Borisov, *Macromolecules*, 1995, **28**, 1491–1499.
[18] E. B. Zhulina and M. Rubinstein, *Soft Matter*, 2012, **8**, 9376–9383.
[19] R. Israëls, F. A. M. Leermakers, G. J. Fleer and E. B. Zhulina, *Macromolecules*, 1994, **27**, 3249–3261.
[20] G. Chen and S. Das, *J. Phys. Chem. B*, 2015, **119**, 12714–12726.
[21] G. Chen and S. Das, *RSC Adv.*, 2015, **5**, 4493–4501.
[22] S. Misra, S. Varanasi and P. P. Varanasi, *Macromolecules*, 1989, **22**, 4173–4179.
[23] G. Chen and S. Das, *J. Phys. Chem. B*, 2016, **120**, 6848–6857.
[24] G. Chen and S. Das, *J. Phys. Chem. B*, 2017, **121**, 3130–3141.
[25] G. Chen, H. S. Sachar and S. Das, *Soft Matt.*, 2018, **14**, 5246–5255.
[26] R.S. Maheedhara, H. S. Sachar, H. Jing and S. Das, *J. Phys. Chem. B*, 2018, **122**, 7450–7461.
[27] P. M. Biesheuvel, W. M. de Vosa and V. M. Amoskov, *Macromolecules*, 2008, **41**, 6254–6259.
[28] J. Patwary, G. Chen and S. Das, *Microfluid. Nanofluid.*, 2016, **20**, 37.
[29] G. Chen and S. Das, *J. Appl. Phys.*, 2015, **117**, 185304.
[30] G. Chen, J. Patwary, H. S. Sachar and S. Das, *Microfluid. Nanofluid.*, 2018, **22**, 112.
[31] E. B. Zhulina and O. V. Borisov, *Langmuir*, 2011, **27**, 10615–10633.
[32] E. B. Zhulina and O. V. Borisov, *J. Chem. Phys.*, 1997, **107**, 5952–5967.
[33] Y. V. Lyatskaya, F. A. M. Leermakers, G. J. Fleer, E. B. Zhulina and T. M. Birshtein, *Macromolecules*, 1995, **28**, 3562–3569.
[34] I. O. Lebedeva, E. B. Zhulina and O. V. Borisov, *J. Chem. Phys.*, 2017, **146**, 214901.
[35] E. B. Zhulina, J. K. Wolterink and O. V. Borisov, *Macromolecules*, 2000, **33**, 4945–4953.
[36] J. P. Mahalik, Y. Yang, C. Deodhar, J. F. Ankner, B. S. Lokitz, S. M. Kilbey II, B. G. Sumpter and R. Kumar, *J. Pol. Sci. B*, 2016, **54**, 956–964.
[37] H. S. Sachar, V. S. Sivasankar and S. Das, *Soft Matter*, 2019, **15**, 559–574.
[38] H. S. Sachar, V. S. Sivasankar and S. Das, *Soft Matter*, 2019, **15**, 5973–5986.
[39] M. S. Kilic, M. Z. Bazant, and A. Ajdari, *Phys. Rev. E*, 2007, **75**, 021502.
[40] B. D. Storey and M. Z. Bazant, *Phys. Rev. E*, 2012, **86**, 056303.

[41] M. Z. Bazant, B. D. Storey and A. A. Kornyshev, *Phys. Rev. Lett.*, 2011, **106**, 046102.
[42] M. McEldrew, Z. A. H. Goodwin, A. A. Kornyshev and M. Z. Bazant, *J. Phys. Chem. Lett.*, 2018, **9**, 5840–5846.
[43] R. P. Misra, S. Das, and S. K. Mitra, *J. Chem. Phys.*, 2013, **138**, 114703.
[44] H. S. Sachar, T. H. Pial, P. R. Desai, S. A. Etha, Y. Wang, P. W. Chung, and S. Das, *Matter* 2020, DOI: 10.1016/*j.matt*.2020.02.022
[45] L. Suo, O. Borodin, T. Gao, M. Olguin, J. Ho, X. Fan, C. Luo, C. Wang and K. Xu, *Science*, 2015, **350**, 938–943.
[46] Yang, C., Chen, J., Qing, T., Fan, X., Sun, W., von Cresce, A., Ding, M. S., Borodin, O., Vatamanu, J., Schroeder, M. A., and Eidson, N. 4.0 V aqueous Li-ion batteries. *Joule*, 2017, **1**, 122–132.
[47] M. V. Fedorov and A. A. Kornyshev, *Chem. Rev.*, 2014, **114**, 2978–3036.
[48] A. A. Kornyshev, *J. Phys. Chem. B*, 2007, **111**, 5545–5557.
[49] Y. Han, S. Huang and T. Yan, *J. Phys. Condens. Matter*, 2014, **26**, 284103.
[50] J. E. Andrews and S. Das, *RSC Adv.*, 2015, **5**, 46873–46880.
[51] J-S. Sin, N-H. Kim and C-S. Sin, *Colloid Surf. A*, 2017, **529**, 972–978.
[52] E. B. Zhulina, V. A. Pryamitsyn and O. V. Borisov, *Pol. Sci. USSR*, 1989, **31**, 205–216.
[53] R. H. Perry, D. W. Green and J. O. Maloney, Perry's chemical engineers' handbook, McGraw-Hill, New York, 1997.
[54] A. T. Celebi, B. Cetin and A. Beskok, *J. Phys. Chem. C*, 2019, **123**, 14024–14035
[55] R. Mancinelli, A. Botti, F. Bruni, M. A. Ricci and A. K. Soper, *J. Phys. Chem. B*, 2007, **111**, 13570–13577.
[56] Y. Marcus, *J. Chem. Phys.*, 2012, **137**, 154501.
[57] A. Poddar, D. Maity, A. Bandopadhyay and S. Chakraborty, *Soft Matter*, 2016, **12**, 5968-5978.